Title

Mapping white matter integrity in elderly people with HIV

Journal

Human Brain Mapping, 35(3)

ISSN

1065-9471

Authors

Nir, Talia M
Jahanshad, Neda
Busovaca, Edgar
et al.

Publication Date

2014-03-01

DOI

10.1002/hbm.22228

Peer reviewed

Mapping White Matter Integrity in Elderly People with HIV

Talia M. Nir,[1] Neda Jahanshad,[1,2] Edgar Busovaca,[3] Lauren Wendelken,[3] Krista Nicolas,[3] Paul M. Thompson,[1]* and Victor G. Valcour[3]

[1]*Imaging Genetics Center, Laboratory of Neuro Imaging, Department of Neurology, UCLA School of Medicine, Los Angeles, California*
[2]*Medical Imaging Informatics Group, Department of Radiology, UCLA School of Medicine, Los Angeles, California*
[3]*Memory and Aging Center, UCSF, San Francisco, California*

Abstract: People with HIV are living longer as combination antiretroviral therapy (cART) becomes more widely available. However, even when plasma viral load is reduced to untraceable levels, chronic HIV infection is associated with neurological deficits and brain atrophy beyond that of normal aging. HIV is often marked by cortical and subcortical atrophy, but the integrity of the brain's white matter (WM) pathways also progressively declines. Few studies focus on older cohorts where normal aging may be compounded with HIV infection to influence deficit patterns. In this relatively large diffusion tensor imaging (DTI) study, we investigated abnormalities in WM fiber integrity in 56 HIV+ adults with access to cART (mean age: 63.9 ± 3.7 years), compared to 31 matched healthy controls (65.4 ± 2.2 years). Statistical 3D maps revealed the independent effects of HIV diagnosis and age on fractional anisotropy (FA) and diffusivity, but we did not find any evidence for an age by diagnosis interaction in our current sample. Compared to healthy controls, HIV patients showed pervasive FA decreases and diffusivity increases throughout WM. We also assessed neuropsychological (NP) summary *z*-score associations. In both patients and controls, fiber integrity measures were associated with NP summary scores. The greatest differences were detected in the corpus callosum and in the projection fibers of the *corona radiata*. These deficits are consistent with published NP deficits and cortical atrophy patterns in elderly people with HIV. *Hum Brain Mapp 35:975–992, 2014.*

Key words: brain integrity; white matter; diffusion tensor imaging; cognition; HIV; cART

INTRODUCTION

Around 30 million people worldwide are living with HIV, and an estimated 2 million new adults become infected each year (UNAIDS, 2010). As combination antiretroviral therapy (cART) is more widely available, people with HIV are living longer (Carpenter et al., 2000; Valcour et al., 2004a; Vance, 2010). However, even when plasma viral load is reduced to untraceable levels, chronic HIV infection can impair neurological function and promote brain atrophy beyond the level characteristic of normal aging (Becker et al., 2011; Heaton et al., 2010; McArthur, 2004; Sacktor et al., 2002).

On average, patients with HIV have greater cortical, subcortical, and cerebellar atrophy than healthy controls (Cohen et al., 2010a; Klunder et al., 2008; Thompson et al., 2005), and greater ventricular expansion, a marker of brain atrophy (Thompson et al., 2006; Wang et al., 2010). Diffuse white matter atrophy may also be found, especially in

*Correspondence to: Paul M. Thompson, Laboratory of Neuro Imaging, UCLA School of Medicine, 635 Charles Young Drive, Los Angeles, CA 90095, USA. E-mail: thompson@loni.ucla.edu

Received for publication 5 March 2012; Revised 2 November 2012; Accepted 5 November 2012

DOI: 10.1002/hbm.22228

Published online 30 January 2013 in Wiley Online Library (wileyonlinelibrary.com).

regions that innervate the atrophic cortical regions (Brun et al., 2007; Chiang et al., 2007; Lepore et al., 2008) and in the corpus callosum (Thompson et al., 2006). Brain atrophy in people with HIV is often associated with psychomotor slowing, executive dysfunction, and impaired working memory and attention (Ances and Ellis, 2007; Becker et al., 1997; Heaton et al., 2011; McArthur et al., 2003). It has been suggested that aging may have an additive or synergistic effect on top of the effect of HIV infection, resulting in a compounded detrimental effect on cognition (Goodkin et al., 2001; Wendelken and Valcour, 2012).

There is growing evidence that both normal aging and HIV-associated neurocognitive impairment share many similarities including executive function deficits and memory dysfunction (Buckner, 2004 ; Glisky, 2007; Hartley, 2006; Kramer et al., 2007; Peavy et al., 1994; Woods et al., 2009). If these effects are additive, they may result in premature or accelerated cognitive difficulties in older HIV+ patients (Brew et al., 2009; Holt et al., 2012). Additionally, atrophy and white matter lesions in both aging and HIV have been shown to preferentially involve fronto-striatal networks (Raz and Rodrigue, 2006; Schouten et al., 2011; Tate et al., 2009; Tucker et al., 2004). There is increasing evidence that the expression and progression of neurodegenerative diseases associated with aging, such as Alzheimer's disease, may be facilitated by HIV resulting in premature brain and cognitive decline (Brew et al., 2009). Comorbidities such as cardiovascular disease, cerebrovascular disease, high cholesterol, and diabetes may also play a role in accelerating brain atrophy, and are more likely to be present in older individuals (Becker et al., 2009; Valcour et al., 2005). While neuropsychological (NP) studies of HIV+ cohorts have found both age and HIV effects, results are mixed, perhaps due to limited power to pick up second order effects. Some studies do not detect any effect of aging on cognitive impairment in HIV (Cysique et al., 2006; Cysique et al., 2011; Valcour et al., 2011) but others report higher rates of impairment by NP testing with increasing age (Cherner et al., 2004; Kissel et al., 2005; Scott et al., 2011). Given the increased life expectancy of HIV infected individuals, studies of older HIV+ adults are particularly important.

Because HIV-related brain changes are not well understood in people over the age of 60 years, we set out to better define and map microstructural white matter alterations, and assess the main systems affected. Here we performed one of the largest neuroimaging studies of elderly HIV patients (over age 60 years). We mapped the profile of white matter fiber integrity based on diffusion tensor images (DTI) in 56 HIV+ patients and 31 controls of similar age and sex. DTI is a variant of MRI that maps white matter integrity based on measures of water diffusion in the brain. Intact white matter axons have highly anisotropic (directionally constrained) water diffusion, as the myelin sheaths tend to block diffusion perpendicular to the axonal trajectory. The most common DTI-derived measure of fiber integrity is fractional anisotropy (FA), followed by mean diffusivity (MD). FA is a scalar value between zero and one that estimates how directionally constrained diffusion is along white matter tracts, thereby indicating fiber coherence, while MD is an overall measure of diffusion in all directions. DTI is sensitive to microscopic white matter injury not always detectable on standard anatomical MRI (Filippi et al., 2001; Pomara et al., 2001). Prior DTI studies of HIV+ patients have found lower FA and increased MD in the corpus callosum and frontal white matter among other regions (Chang et al., 2008; Cloak et al., 2004; Filippi et al., 2001; Pfefferbaum et al., 2007; Thurnher et al., 2005; Wu et al., 2006).

To our knowledge, no published studies have examined elderly HIV+ cohorts over the age of 60 years, where normal aging may influence the deficit pattern of HIV infection. Using 3D statistical maps, we set out to (1) define the profile of differences in white matter microstructure in elderly HIV patients on stable cART versus matched controls, (2) locate associations between global NP scores and white matter microstructure, and (3) examine any interaction of age, within this narrow but older age group, with HIV infection. We hypothesized that older HIV patients would have lower white matter FA, as well as higher mean, radial, and axial diffusivity in the majority of the white matter, as nearly all major regions of the brain show atrophy and many have been implicated in DTI studies of HIV. However, the white matter of the frontal lobe, including the fronto-striatal connections, were of special interest as they have been shown to be especially atrophied in both prior HIV and aging studies. We expected that similar regions would be implicated in older patients compared to younger ones, but we predicted that the effect sizes for measures of brain deterioration may be greater in older people, perhaps simply because they have been ill for longer.

METHODS

Clinical Sample

MRI, DTI, clinical, and NP data were collected from HIV-infected participants enrolling in a larger longitudinal study of HIV, aging and cognition at the Memory and Aging Center, UCSF. All participants were ambulatory and responded to advertisements for an HIV cognitive study or were referred by clinicians. Participants were recruited regardless of cognitive symptoms. Individuals with learning disabilities, major psychiatric or neurological illness, current or past brain infection, major systemic illness or head injury with cognitive sequelae were excluded. Subjects were scanned at 3 Tesla (with the protocol below) at their first research visit (baseline, $n = 42$) or at the 1-year follow-up visit ($n = 14$), resulting in 52 male and two female cases between the ages of 60 and 70 years, and two male cases between the ages of 70 and 80 years. A fasting blood draw was collected for each HIV+ subject within 3 months of the MRI acquisition. Clinical HIV parameters

TABLE I. Characteristics of seronegative controls and HIV+ subjects

	Controls ($n = 31$)	HIV+ ($n = 56$)	P-value (Controls vs. HIV+)
Age (years)	65.4 ± 2.2	63.9 ± 3.7	0.056
Sex	27 Male/4 Female	54 Male/2 Female	–
Education (years)	17.5 ± 2.1	16.1 ± 2.2	0.005
CD4 (count/mm^3)	–	520.0 ± 218.0[a]	–
Nadir CD4 (count/mm^3)	–	205.5 ± 188.4[b]	–
Viral load (copies/mL)	–	334.6 ± 1106.6[a]	–
Log viral load (copies/mL)	–	1.9 ± 0.5[a]	–
Duration of HIV infection (years)	–	20.0 ± 6.4	–
Individuals on cART	–	53	–

[a] $n = 53$.
[b] $n = 54$.

(CD4 count and plasma HIV RNA levels) were captured through clinical reports or standard laboratory testing within three months of their research visit. All but six patients had undetectable plasma HIV RNA (defined as <400 copies/mL). Duration of HIV infection and CD4 nadir were self-reported. Although not a requirement of the study, all but three subjects were on cART at the time of cognitive assessment (Table I).

HIV-negative control subjects of similar age and sex were selected from existing healthy aging cohorts at UCSF and all underwent the same neurological, NP (except grooved pegboard testing and finger tapping), and imaging protocols as the HIV+ subjects. These individuals had similarly responded to public recruiting advertisements and were evaluated by clinicians where they were deemed to have normal cognition. The controls were selected by including all available HIV-negative healthy aging male subjects between ages 60 and 70 years and four randomly selected female subjects. Strictly speaking, the HIV+ patient group was not older than the controls (Table I; $P = 0.056$). The study was approved by the Medical Institutional Review Boards (IRBs) of the University of California at San Francisco and of the UCLA School of Medicine. All participants provided informed written consent.

We adopted the NP testing battery in the national Uniform Data Set (UDS) of the Alzheimer's Disease Research Centers (ADRC, National Institute on Aging/NIH) since all cases were co-enrolled into the ADRC at the UCSF Memory and Aging Center (MAC) as an "at-risk" group for neurodegenerative disorders. The UDS has published tables of control group means and standard deviations (SD, $n = 2143$) by age decade, allowing calculation of standardized z-scores for each individual's performance using standard techniques ((subject raw score — age-group mean score)/age-group SD; Weintraub et al., 2009). Included in the UDS is a declarative memory task (the Logical Memory A immediate and delayed trials, "Story Recall"), Digit Span Forward and Backward, category fluency for animals, the Trail Making A and Trail Making B tasks, and the Wechsler Adult Intelligence Scale (WAIS) Digit Symbol task. We added the following tests to allow a more global characterization of cognition: the Benson Figure Copy and Recall tests, an internally developed and normed visuospatial and visual recall task that is a simplification of the Rey Complex Figure (Possin et al., 2011); an internally developed and normed modified trails (set shifting) task alternating numbers to days of the week (Kramer et al., 2003), the STROOP Interference test (Heflin et al., 2011), the Visual Object and Space Perception Battery: Number Location (VOSP; Rapport et al., 1998), the Grooved Pegboard test in dominant and non-dominant hands (Ruff and Parker, 1993), the Finger Tapping test in dominant and non-dominant hands (Ruff and Parker, 1993), and three scores of the California Verbal Learning Test — II (CVLT-II, 16 item) test — trials 5, immediate recall and delayed recall. To assess depressive symptoms we used the 30-item Geriatric Depression Scale (GDS). For all tests, standardized z-scores were calculated using published normative data, and when published normative data were unavailable MAC-developed normative data were used (Benson Figure and Modified Trails). Although published normative data exist for the Grooved Pegboard, we used internal normative data ($n = 38$) since published normative data for this age group identified an unacceptable number of impaired subjects (≥1SD below the norm) in our control cases. For all other tests, the distribution was acceptable to combine as an arithmetic average summary score (NPZ-global). For comparisons between HIV+ and HIV-negative groups, we also created an abbreviated (short) summary score (sNPZ) that did not include the finger tapping and grooved pegboard tests, since these were not completed in most of our HIV-negative controls.

MRI and DTI Scanning

All subjects underwent whole-brain MRI scanning on a Siemens 3 Tesla TIM Trio scanner with a 12-channel head coil. T1-weighted MP-RAGE sequences (240 × 256 matrix; FOV = 256mm; 160 slices; voxel size = 1.0 × 1.0 ×1.0 mm^3; TI = 900 ms; TR = 2300 ms; TE = 2.98 ms; flip angle = 9°) and diffusion MRI (dMRI) sequences for diffusion tensor

imaging (DTI) analysis (100 ×100 matrix; FOV = 220 mm; 55 slices; voxel size = 2.2 × 2.2 × 2.2 mm^3; TR = 8000 ms; TE = 109 ms) were collected. Sixty-five separate images were acquired for each subject's scan: one T2-weighted image with no diffusion sensitization (also known as a b_0 image) and 64 diffusion-weighted images (DWI; b = 2000 s/mm^2). We note briefly that we used a slightly higher *beta*-value in this study than is typical in many clinical DTI studies that use a value of 1000 s/mm^2. In prior work, we evaluated the benefits of using a higher *beta*-value — or even multiple *beta*-values at once — (Zhan et al., 2011), and found relative enhancement of diffusion along axonal fibers at higher *beta*-values, and relative suppression of random non-axonal diffusion (see related work on CHARMED, by Assaf and Basser, 2005 and DSI, by Wedeen et al., 2005). The higher *beta*-value in this study should not have affected the diffusivity measures substantially. All DWI and T1-weighted MR images were quality checked visually to exclude scans with excessive motion and/or artifacts.

Image Analysis

Preprocessing steps

For each subject, all raw DWI volumes were aligned to the b_0 image (DTI volume with no diffusion sensitization) using the FSL "eddy-correct" tool (www.fmrib.ox.ac.uk/fsl) to correct for head motion and eddy current distortions. All extra-cerebral tissue was subsequently removed from the T1-weighted anatomical scans using ROBEX, an automated brain extraction program trained on manually "skull-stripped" MRI data from hundreds of healthy young adults (Iglesias et al., 2011). Non-brain tissue was also removed from the DWI using the Brain Extraction Tool from FSL (Smith, 2002). Anatomical scans subsequently underwent intensity inhomogeneity normalization using the MNI "nu_correct" tool (www.bic.mni.mcgill.ca/software/). To align data from different subjects into the same 3D coordinate space, each T1-weighted anatomical image was linearly aligned to a standard brain template (the Colin27; Holmes et al., 1998) using FSL's FLIRT (Jenkinson et al., 2002) with 9 degrees of freedom to allow translations, rotations and scaling in 3D. To correct for echo-planar imaging (EPI) induced susceptibility artifacts, which can cause distortions at tissue-fluid interfaces, skull-stripped b_0 images were linearly aligned and then elastically registered to their respective T1-weighted structural scans using an inverse consistent registration algorithm with a mutual information cost function (Leow et al., 2007; Jahanshad et al., 2010). The resulting 3D deformation fields were then applied to the remaining 64 DWI volumes prior to mapping diffusion parameters.

DTI maps

A single diffusion tensor (Basser et al., 1994), or ellipsoid, was modeled at each voxel in the brain from the eddy- and EPI-corrected DWI scans using FSL, and scalar anisotropy and diffusivity maps were obtained from the resulting diffusion tensor eigenvalues (λ_1, λ_2, λ_3) which capture the length of the longest, middle, and shortest axes of the ellipsoid. FA, a measure of the degree of diffusion anisotropy, was calculated from the standard formula:

$$FA = \sqrt{\frac{3}{2}}\frac{\sqrt{(\lambda_1 - <\lambda>)^2 + (\lambda_2 - <\lambda>)^2 + (\lambda_3 - <\lambda>)^2}}{\sqrt{\lambda_1^2 + \lambda_2^2 + \lambda_3^2}} \in [0, 1]$$

$$<\lambda> = \frac{\lambda_1 + \lambda_2 + \lambda_3}{3}$$

where $<\lambda>$ is the MD, or average degree of diffusion across all directions. Radial diffusivity (RD) captures the average diffusivity perpendicular to axonal fibers, and was calculated as the average of the two smallest eigenvalues:

$$RD = \frac{\lambda_2 + \lambda_3}{3}$$

Axial diffusivity is defined as the primary (largest) eigenvalue (AD = λ_1), and captures the longitudinal diffusivity or the component of diffusivity parallel to axonal fibers.

Template creation and spatial normalization

A study-specific minimal deformation template (MDT; Gutman et al., 2010) was created using 31 control and 31 HIV+ spatially aligned FA maps (N-total = 62). Using a customized template from subjects in the study (rather than a standard atlas or a single optimally chosen subject) can reduce bias in the registrations and improve registration accuracy (Gutman et al., 2010). The MDT is the template that deviates least from the anatomy of the subjects, and has been shown to improve statistical power (Lepore et al., 2007). The MDT was generated by creating an initial affine mean template from all 62 subjects, then registering all the aligned individual scans to that mean using a fluid registration based on the registration algorithm developed by Leow et al. (2007) while regularizing the Jacobians (Yanovsky et al., 2007). A new mean was created from the registered scans; this process was iterated several times. Each subject's initial FA map was elastically registered to the final MDT and the resulting deformation fields were applied to the three diffusivity maps to align them to the same coordinate space. To ensure white matter alignment across subjects, registered FA maps were thresholded at FA > 0.2 to include only highly anisotropic anatomy and elastically registered to the thresholded MDT (FA > 0.2). Again, the resulting deformation fields were applied to all four previously registered DTI maps.

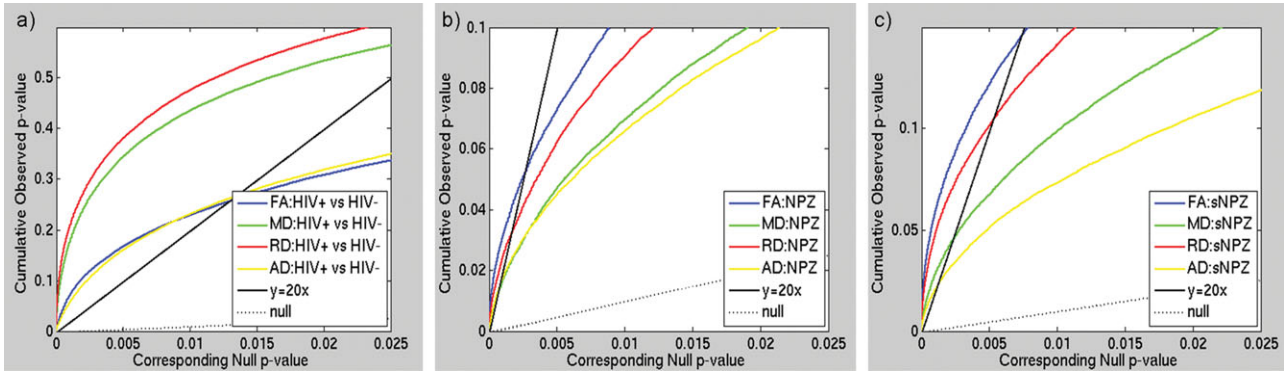

Figure 1.

FA, MD, RD, and AD analyses in HIV+ patients and controls. Here we show cumulative distribution function (CDF) plots of the distribution of the *P*-values obtained from voxel-wise linear regressions, which are subjected to multiple comparisons correction using standard FDR (Benjamini and Hochberg, 1995). (**a**) When comparing HIV+ patients to controls, the RD effects were much greater as denoted by the higher critical *P*-values controlling the FDR (i.e., the highest non-zero *x*-coordinate where the CDF crosses the $y = 20x$ line). When examining NPZ (**b**) and sNPZ (**c**) correlations, effects on FA were the greatest, followed by RD. These distributions were obtained from highly anisotropic white matter in voxels within the boundaries of the MDT mask thresholded at FA > 0.2 where the power is greater to detect differences. All anisotropy and diffusivity maps show FDR significant results. [Color figure can be viewed in the online issue, which is available at wileyonlinelibrary.com.]

Partial volume compensation

Point-by-point comparisons of DTI scans may be complicated by the fact that voxels at structure boundaries (such as the ventricles) may contain different proportions of white matter (WM), even after careful registration; this partial volume effect can lead to differences in fiber integrity measures that are in fact due to misregistrations of structure interfaces across subjects. To address this, Lee et al. (2009) advocated a partial volume compensation method using a tissue-specific, smoothing-compensated "T-SPOON" method for voxel based analyses to improve tissue specificity and adjust for image misregistration. The final spatially normalized FA maps were thresholded at FA > 0.2 and binarized to create a WM mask for each subject. The mask was then applied to all four DTI maps. Each subject's binarized WM mask and masked DTI maps were smoothed with a Gaussian kernel (5 mm FWHM), and each smoothed DTI map was subsequently divided by the smoothed WM mask. Typically, images are simply co-registered and then smoothed to compensate for image misregistration and to improve the signal-to-noise ratio. In this case we smooth both a WM mask and DTI map. Since both images are blurred to the same extent, their division will make the smoothed data have values more similar to the original data, and can be considered a kind of adjustment for misregistration. When compared to conventional voxel-based analysis (VBA) methods, the "T-SPOON" method is better able to suppress false positives in the group analyses by compensating for image misregistration via smoothing (Lee et al., 2009).

Statistical Analyses

We ran linear regressions, voxel-wise, adjusting for sex and age, to test for statistical effects of HIV diagnosis in the entire study population ($n = 87$) on white matter integrity as determined by each of FA, MD, RD, and AD. We additionally tested for correlations between these DTI measures and global NP summary *z*-scores (NPZ) in HIV+ subjects, adjusting for sex and age ($n = 56$), as well as the effects of an abbreviated global sNPZ in the entire study population, including HIV+ patients and controls ($n = 87$), adjusting for sex, age, and diagnostic status. A final linear regression was performed to test for an interaction between age and HIV diagnosis, simultaneously adjusting for the linear effects of age, sex, and diagnostic status. To limit statistical testing to highly anisotropic white matter, where the power is greater to detect differences, statistics were only run on voxels within the boundaries of the MDT mask thresholded at FA > 0.2. To visualize effect sizes in the anisotropy and diffusivity maps, we computed and graphed the cumulative distribution function (CDF) of the *P*-values obtained from the voxel-wise linear regressions (Fig. 1). The *P*-values were plotted against their expected null distribution. Computing thousands of association tests on a voxel-wise level can introduce a high false positive error rate in neuroimaging studies. To correct for these errors, the maps must still be significant after standard false discovery rate correction (FDR; Benjamini and Hochberg, 1995). If there are no group differences (a null distribution), then the plot would fall approximately along the $y = x$ line. However, if the CDF initially rises at a rate steeper than 20 times the null CDF ($y = 20x$), then the

corresponding maps are FDR significant at $q = 0.05$. The larger the deviation is from this line, the larger the effect sizes. As all maps passed standard FDR, we also used the searchlight method for FDR correction (Langers et al., 2007) to get a more comprehensive regional significance. All statistical maps (Figs. 2–4) were thresholded at the corrected *P*-value of 0.05 to show regression coefficient values only in regions that controlled the searchlight false discovery rate. The resulting significant correlations either have positive or negative effects, dependant on the slope of the regression (*beta*).

Post hoc Statistical Analyses

Referring findings to a white matter tract atlas

In a *post hoc* analysis, we set out to better localize our pervasive findings and elastically registered (Leow et al., 2007) the FA image from the JHU DTI atlas (Mori et al., 2008) to our MDT, as previously described in section "Template Creation and Spatial Normalization" for an individual subject. We then applied that deformation to the stereotaxic WM atlas labels, using nearest neighbor interpolation to avoid intermixing of labels. This placed the atlas regions of interest (ROIs) in the same coordinate space as our individual images. We were then able to calculate the average FA, MD, RD, and AD within the boundaries of each of the ROIs for each subject. We assessed 49 of the 50 total possible atlas ROIs (Table II), excluding the fornix as it is small and prone to misregistration (Kuroki et al., 2006; Lee et al., 2012). As noted in Kuroki et al. (2006), any measures derived from the fornix can be prone to errors as they would have to rely on aligning a segmented atlas template to a region that is rather small, possibly identifying different anatomy in different subjects. As the fornix is thin and surrounded by CSF, partial voluming is a problem and any DTI-derived values would tend to reflect the fraction of CSF in the voxel rather than the intrinsic diffusion parameters of the fornix. We ran linear regressions on the 49 average anisotropy and diffusivity measures within the 49 ROIs, again adjusting for sex and age, to test for statistical effects of HIV diagnosis and NPZ score (in HIV+ subjects only). We used the standard false discovery rate procedure to control the false positive rate at $q = 0.05$ (Benjamini and Hochberg, 1995). Table III reports the unnormalized *beta*-values for each of the ROI atlas average anisotropy and diffusivity analyses.

Nadir and current CD4 T-cell count, and duration of HIV infection

We further assessed whether white matter integrity in the patient group was related to measures of the severity of HIV infection. We ran voxel-wise linear regressions, adjusting for sex and age, to test for any statistical effects of nadir and current CD4 T-cell count, and HIV infection duration on anisotropy and diffusivity maps within the boundaries of the MDT mask thresholded at FA > 0.2. We used the searchlight method for FDR correction (Langers et al., 2007).

RESULTS

White Matter Integrity in HIV+ Versus Healthy Controls

Compared to healthy controls, HIV+ patients showed pervasive deficits in fiber integrity, as measured by the standard measure FA throughout the entire brain (corrected $P < 0.05$; Langers et al., 2007; Fig. 2a). The most prominent FA deficits were detected in the genu, body and splenium of the corpus callosum (CC; FA was lower by up to 0.045 units, on average, in the body of the corpus callosum; FA values can in theory range between 0 and 1). Deficits extended through commissural fibers, including the right *tapetum* of the CC, and projection fibers throughout the anterior, superior and posterior *corona radiata*. FA reductions were also detected bilaterally in the white matter of the frontal gyri. Lower FA was observed bilaterally in projection fibers including the anterior limbs of the internal capsules, which continue into the association fibers of the superior fronto-occipital fasciculi (SFO), and in the retrolenticular internal capsules, continuing bilaterally into the posterior limbs. The internal capsule projections converge into the cerebral peduncles, which also showed decreased FA in the HIV+ group. The HIV+ group also showed bilateral FA reductions in the posterior thalamic radiation/optic radiation projection fibers (FA reduced up to 0.047 units), in the thalamus, and throughout the occipital gyri. Long association fibers including the left uncinate fasciculus the superior longitudinal fasciculi (SLF) and the external capsules showed FA decreases bilaterally, as did association fibers in the limbic system. These included parts of the cingulum and the left *stria terminalis/crus* of the fornix. The white matter in the temporal gyri, including the temporal lobe sagittal stratum which carries the long association fibers of the inferior longitudinal and inferior fronto-occipital fasciculi (ILF and IFO), was affected in both hemispheres, as was the angular/supramarginal gyrus and parietal lobule. Deficits were also found in the inferior cerebellar peduncles, pontine tracts, medial lemniscus, and the left superior cerebellar peduncle.

This pattern of significance was largely replicated for the three diffusivity measures. As predicted, we found higher MD, RD, and AD values in HIV+ patients relative to controls (Fig. 2b–d) and the effects were larger and even more diffuse.

These pervasive results in all four DTI maps were corroborated by the JHU atlas results: 31 out of 49 regions showed significant FA deficits, 41 regions MD deficits, 43 regions RD deficits, and 27 regions showed significant AD deficits (Table III). In all four maps, the body and splenium of the CC, superior *corona radiata*, and external

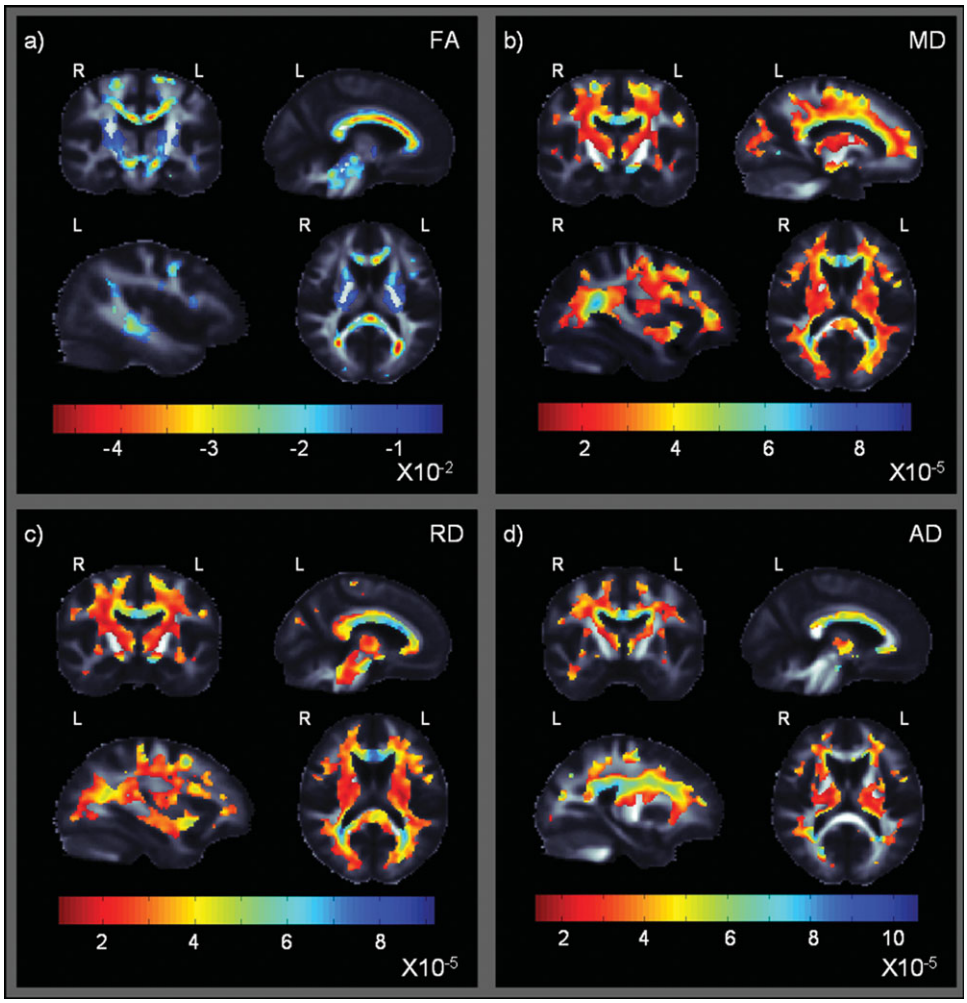

Figure 2.

Statistical maps show where HIV+ patients differ from controls in their fractional anisotropy (**a**), and mean, radial and axial diffusivity (**b–d**). Rather than show *P*-values for the group differences, which are higher where FA is higher, these maps show *beta*-values (non-normalized slope of the regression, representing the mean group difference in each imaging measure) within regions with significant differences between HIV+ patients and healthy controls (corrected $P < 0.05$; Langers et al., 2007). Both larger negative FA *beta*-values — shown in (a) in red — and larger positive MD, RD, and AD *beta*-values — shown in (b–c) in blue — suggest a decrease in fiber integrity in HIV+ relative to controls. Prominent differences were found in the corpus callosum, and in projection fibers extending throughout the *corona radiata*. [Color figure can be viewed in the online issue, which is available at wileyonlinelibrary.com.]

capsules were among the regions that showed the most significant differences. MD, RD, and AD ROIs also revealed significant deficits in the right *tapetum*, and the inferior fronto-occipital fasciculus. Reductions in mean FA were found in the left cingulum (hippocampus), the cerebral peduncles, medial lemniscus, and left inferior and superior cerebellar peduncles.

Correlation with Neuropsychological Scores

Figure 3 shows WM regions where FA and diffusivity differences correlated with the short global NP summary *z*-scores (sNPZ) in the entire study population, including both HIV+ patients and controls ($n = 87$; corrected $P < 0.05$; Langers et al., 2007). This suggests that global NP *z*-scores calculated are a viable tool to detect cognitive associations. Correlations were in the expected direction, as deteriorations in fiber integrity are generally accompanied by lower FA and higher diffusivity values.

Figure 4 further shows DTI-based associations with the global NP summary *z*-scores (NPZ), which includes manual dexterity tasks, in HIV+ patients only ($n = 56$; corrected $P < 0.05$; Langers et al., 2007). Associations were in the expected direction, with impaired fiber integrity in

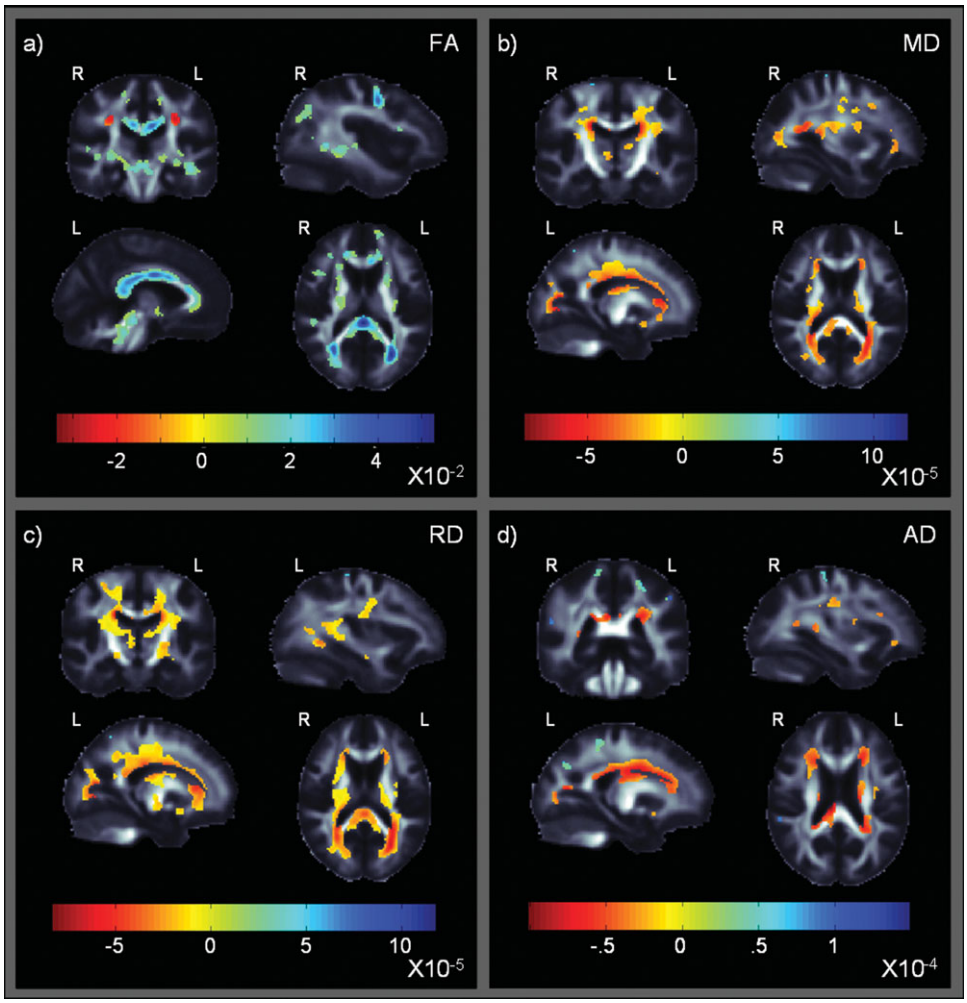

Figure 3.

These maps show that cognitive performance is related to detectable differences in fractional anisotropy (**a**), and mean, radial, and axial diffusivity (**b–d**) in the entire cohort, including both HIV+ patients and controls. These maps show *beta*-values (non-normalized slope of the regression in units of imaging measure per unit difference in cognitive z-scores) within regions that significantly correlate with the short global NP summary z-scores (sNPZ) in HIV+ and controls (corrected $P < 0.05$; Langers et al., 2007). The most notable differences were found in the corpus callosum and projection fibers extending throughout the *corona radiata.* Radial diffusivity shows widespread and robust associations, but all maps are significant after multiple comparisons correction via the searchlight FDR method. [Color figure can be viewed in the online issue, which is available at wileyonlinelibrary.com.]

those with poorer performance, as indexed by FA. Positive associations between FA and cognitive measures (Fig. 4a) were detected in the genu, body and most saliently in the splenium of the CC (FA loss of up to 0.059 units with each standard deviation reduction in NPZ in this region) and extended bilaterally into the *tapetum* of the CC. The positive association extended bilaterally through projection fibers in the posterior, superior, and anterior *corona radiata.* Correlations between test performance and fiber integrity were also found in the frontal gyri. Projection fibers also showed similar associations, including the anterior limb of the internal capsule and the left posterior limb which extended into the left retrolenticular internal capsule. Internal capsule projections converge into the midbrain and cerebral peduncles, and these also showed a positive correlation between test performance and fiber integrity. Associations were also found in posterior thalamic radiation projection fibers (including the optic radiation), and in the thalamus and occipital gyri. Limbic association fibers also exhibited FA associations with cognitive performance in bilateral parts of the cingulum/cingulate gyrus, the *crus* of the fornix/*stria terminalis* and the left external capsule.

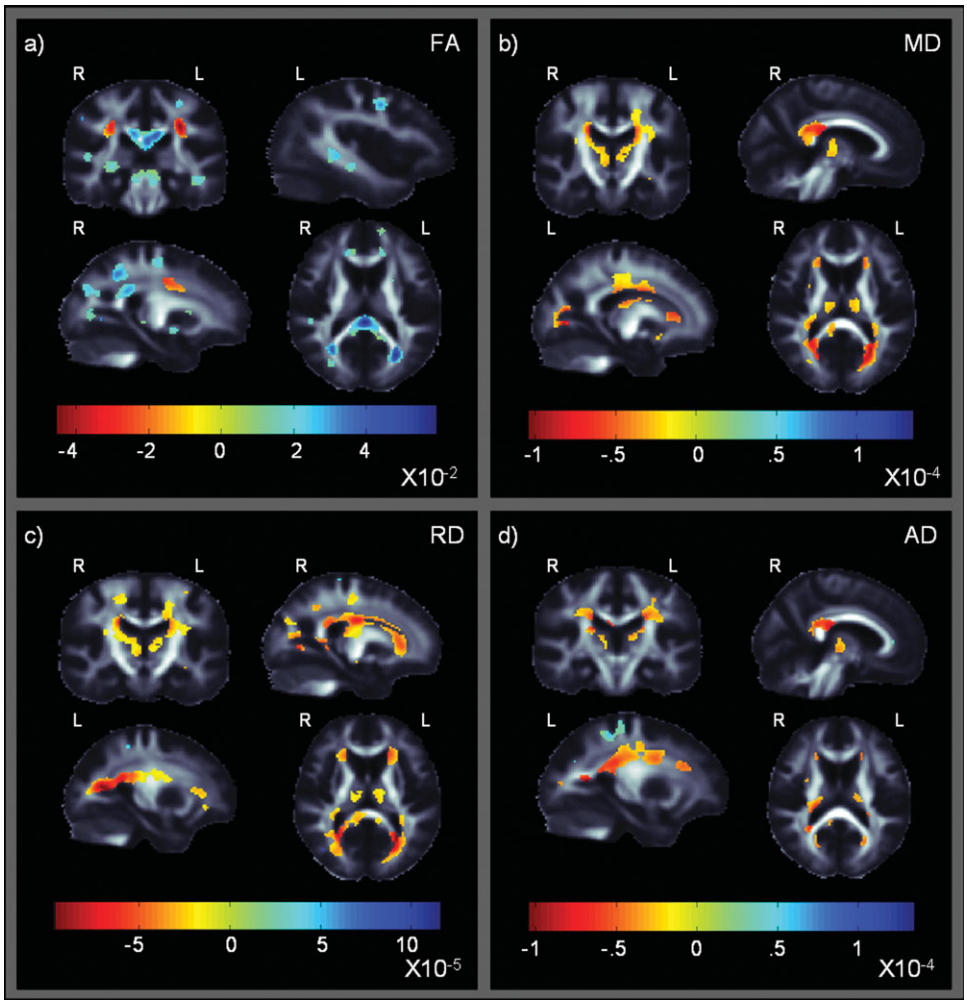

Figure 4.

These maps show *beta*-values of significant associations between diffusion measures and the global NP summary z-scores (NPZ) in HIV+ patients (searchlight corrected $P < 0.05$; Langers et al., 2007). They are similar to those in Figure 2, but with a more general measure of cognitive performance. Strong associations are found in the corpus callosum, and commissural fibers extending throughout the *corona radiata*. (**a**) Areas of significance in FA; (**b–d**) Areas of significance in MD, RD, and AD, respectively. [Color figure can be viewed in the online issue, which is available at wileyonlinelibrary.com.]

The temporal lobe sagittal stratum, which includes the ILF and IFO association fibers, posterior projection fibers and CC splenium commissural fibers, showed FA increases on the right. Better NP testing performance correlated with higher FA in the right temporal gyrus. A positive association was found around the superior parietal lobule/precuneus region in both hemispheres. Bilateral white matter associations were found around the brainstem in the superior cerebellar peduncles and the medial lemniscus.

As hypothesized, we also found a negative association between all three diffusivity measures, RD, MD, AD (Fig. 4b–d respectively), and the NPZ score in HIV patients. In general, these diffusivity measures were all higher — suggesting impairment — in those with poorer cognitive performance. The pattern of associations for all three diffusivity maps essentially resembled that of FA, but, in the opposite direction (this is to be expected as diffusivity is often higher when FA is lower). This negative correlation was found bilaterally throughout commissural, association and projection fibers in the frontal, parietal, occipital, and temporal lobes. We found the most widespread negative association with RD maps, followed by the MD maps. Only weaker associations were found for AD.

The ROI analysis only revealed significant associations between NPZ and average FA and RD (Table III). Both FA and RD showed associations with cognitive scores in the

TABLE II. Index of ROIs from the WM tract atlas (Mori et al., 2008) followed by the abbreviation

Middle cerebellar peduncle	MCP	Superior *corona radiata*	SCR L,R
Pontine crossing tract	PCT	Posterior *corona radiata*	PCR L,R
Genu of corpus callosum	GCC	Posterior thalamic radiation	PTR L,R
Body of corpus callosum	BCC	Sagittal stratum	SS L,R
Splenium of corpus callosum	SCC	External capsule	EC L,R
Corticospinal tract	CST L,R	Cingulum (cingulate gyrus)	CGC L,R
Medial lemniscus	ML L,R	Cingulum (hippocampus)	CGH L,R
Inferior cerebellar peduncle	ICP L,R	Fornix (*crus*)/*Stria terminalis*	FX/ST L,R
Superior cerebellar peduncle	SCP L,R	Superior longitudinal fasciculus	SLF L,R
Cerebral peduncle	CP L,R	Superior fronto-occipital fasciculus	SFO L,R
Anterior limb of internal capsule	ALIC L,R	Inferior fronto-occipital fasciculus	IFO L,R
Posterior limb of internal capsule	PLIC L,R	Uncinate fasciculus	UNC L,R
Retrolenticular part of internal capsule	RLIC L,R	*Tapetum*	TAP L,R
Anterior *corona radiate*	ACR L,R		

splenium and left posterior thalamic radiation. RD additionally showed associations in the *tapetum*, while FA showed associations in the left sagittal stratum and inferior cerebellar peduncle, and bilaterally in the medial lemniscus.

In all four DTI maps, several significant regions exhibited associations in a direction opposite to what would traditionally be accepted as showing impairment. We found regions where test performance was negatively correlated with FA and positivity correlated with the diffusivity measures. To make sure that these results were not false positives we re-ran searchlight FDR (Langers et al., 2007) only on regions that exhibited this opposite association (i.e. for FA, we ran searchlight FDR only on voxels negatively associated with NPZ) and still found a significant association (corrected $P < 0.05$; Langers et al., 2007). These regions were largely found at the junction of the corpus callosum commissural fibers and *corona radiata*. For example, Figures 3a and 4a show a negative association between FA and cognitive score (red regions). Such regions are notorious for fiber crossings which can artificially reduce FA and increase diffusivity when estimated using the "single-tensor" diffusion model (Oishi et al., 2011). This pattern has been found in other studies of elderly patients with a neurodegenerative disorder, and may reflect a selective sparing or selective degeneration of one of the pathways in a region of crossing fibers (Douaud et al., 2011).

HIV and Age Effects

We found no significant HIV diagnosis by age interactions in any of the diffusivity and anisotropy maps. However, age independently and significantly contributed to the models for both NP scores (NPZ and sNPZ), and diagnostic status. As expected, age was significantly negatively associated with FA, and positively associated with diffusivity across all three models (corrected $P < 0.05$; Langers et al., 2007), indicating increasing WM impairment with age. Figure 5 shows ROIs from the WM atlas that were either significantly associated with the age component, the HIV diagnosis component, or associated with both across any of the DTI measures.

To further localize the differences between age related white matter deficits (Table IV) and those related to HIV infection (Table V) we assessed the top 10 most significant regions from the ROI HIV diagnosis analysis. Age had a smaller effect size than HIV status and was not significantly associated with FA in any of the ROIs. In the model, both age and HIV infection were associated most significantly with increased diffusivity measures in the left external capsule, superior longitudinal fasciculus, inferior fronto-occipital fasciculus, and posterior *corona radiata*. HIV infection was also associated with diffusivity measures in the right inferior fronto-occipital fasciculus and posterior *corona radiata*, as well as the body and splenium of the CC, bilateral superior *corona radiata* and cerebral peduncles, and the right posterior thalamic radiation, superior fronto-occipital fasciculus, and *tapetum*. Age, by contrast, was most associated with deficits in the genu of the CC, bilaterally in the anterior *corona radiata* and anterior limb of the internal capsule, and the left fornix (*crus*)/*stria terminalis* region, retrolenticular part of the internal capsule, superior fronto-occipital fasciculus, and uncinate fasciculus.

Nadir and Current CD4 T-cell Count and Duration of HIV Infection

In a *post hoc* analysis, we set out to determine whether white matter integrity, in the patient group, was related to measures of the severity of HIV infection. We detected no significant correlation between duration of infection, CD4, or nadir CD4 count and white matter atrophy for any of the anisotropy and diffusivity measures.

TABLE III. Atlas ROI average anisotropy and diffusivity analyses *beta*-values

	beta-Values Controls vs. HIV+				NPZ in HIV+			
	FA	MD	RD	AD	FA	MD	RD	AD
ROI[a]	$P_{c\text{-}FDR}$[c] = 2.97×10^{-2}	$P_{c\text{-}FDR}$[c] = 3.96×10^{-2}	$P_{c\text{-}FDR}$[c] = 2.62×10^{-2}	$P_{c\text{-}FDR}$[c] = 2.35×10^{-2}	$P_{c\text{-}FDR}$[c] = 5.93×10^{-3}	–	$P_{c\text{-}FDR}$[c] = 3.60×10^{-3}	–
MCP	-2.28×10^{-3}	1.26×10^{-5}	1.09×10^{-5}	1.60×10^{-5}	4.83×10^{-3}[b]	-5.50×10^{-6}	-6.72×10^{-6}	-3.07×10^{-6}
PCT	-1.02×10^{-2} [b]	1.71×10^{-5} [b]	1.72×10^{-5} [b]	1.70×10^{-5}	6.65×10^{-3}[b]	-8.27×10^{-6}	-8.91×10^{-6}	-6.98×10^{-6}
GCC	-1.98×10^{-2} [b]	3.93×10^{-5} [b]	4.13×10^{-5} [b]	3.51×10^{-5} [b]	1.64×10^{-2} [b]	-1.19×10^{-5}	-1.96×10^{-5} [b]	3.51×10^{-6}
BCC	-2.52×10^{-2} [b]	5.13×10^{-5} [b]	5.17×10^{-5} [b]	5.05×10^{-5} [b]	1.45×10^{-2} [b]	-1.07×10^{-5}	-1.72×10^{-5}	2.24×10^{-6}
SCC	-2.06×10^{-2} [b]	3.89×10^{-5} [b]	3.97×10^{-5} [b]	3.72×10^{-5} [b]	2.04×10^{-2} [b]	-2.84×10^{-5}	-3.34×10^{-5} [b]	-1.84×10^{-5}
CST L	-1.19×10^{-2}	2.52×10^{-5} [b]	2.38×10^{-5} [b]	2.79×10^{-5} [b]	-7.84×10^{-4}	-5.58×10^{-6}	-4.47×10^{-6}	-7.81×10^{-6}
ML L	-1.87×10^{-2} [b]	1.65×10^{-5}	2.10×10^{-5} [b]	7.35×10^{-6}	1.47×10^{-2}	-8.62×10^{-6}	-1.41×10^{-5}	2.27×10^{-6}
ML R	-1.58×10^{-2} [b]	1.37×10^{-5}	1.78×10^{-5} [b]	5.55×10^{-6}	1.34×10^{-2}	-6.15×10^{-6}	-1.20×10^{-5}	5.54×10^{-6}
ICP L	-1.25×10^{-2} [b]	1.40×10^{-5} [b]	1.74×10^{-5} [b]	7.20×10^{-6}	1.24×10^{-2}	-1.16×10^{-5}	-1.32×10^{-5}	-8.30×10^{-6}
SCP L	-1.55×10^{-2} [b]	2.04×10^{-5} [b]	2.47×10^{-5} [b]	1.19×10^{-5}	9.42×10^{-3}	-1.08×10^{-5}	-1.45×10^{-5}	-3.48×10^{-6}
CP L	-1.78×10^{-2} [b]	2.77×10^{-5} [b]	2.84×10^{-5} [b]	2.65×10^{-5}	7.90×10^{-3}	-1.25×10^{-6}	-4.91×10^{-6}	6.06×10^{-6}
CP R	-1.72×10^{-2} [b]	2.38×10^{-5} [b]	2.52×10^{-5} [b]	2.09×10^{-5}	1.05×10^{-2}	-2.36×10^{-6}	-6.84×10^{-6}	6.58×10^{-6}
ALIC L	-1.18×10^{-2} [b]	2.46×10^{-5} [b]	2.49×10^{-5} [b]	2.39×10^{-5} [b]	6.94×10^{-3}	-1.62×10^{-5}	-1.72×10^{-5}	-1.43×10^{-5}
ALIC R	-1.10×10^{-2} [b]	2.34×10^{-5} [b]	2.29×10^{-5} [b]	2.45×10^{-5} [b]	5.49×10^{-3}	-1.30×10^{-5}	-1.32×10^{-5}	-1.27×10^{-5}
PLIC L	-7.70×10^{-3}	1.44×10^{-5} [b]	1.32×10^{-5} [b]	1.69×10^{-5}	7.66×10^{-3}	-6.98×10^{-6}	-8.07×10^{-6}	-4.79×10^{-6}
PLIC R	-8.12×10^{-3}	1.51×10^{-5} [b]	1.37×10^{-5} [b]	1.78×10^{-5}	6.34×10^{-3}	-2.96×10^{-6}	-5.69×10^{-6}[b]	2.46×10^{-6}
RLIC L	-9.80×10^{-3} [b]	2.15×10^{-5} [b]	2.13×10^{-5} [b]	2.17×10^{-5} [b]	6.96×10^{-3}	-9.95×10^{-6}	-1.11×10^{-5} [b]	-7.58×10^{-6}
RLIC R	-5.55×10^{-3}	1.99×10^{-5} [b]	1.80×10^{-5} [b]	2.35×10^{-5} [b]	3.85×10^{-3}	-1.53×10^{-5}	-1.41×10^{-5}	-1.76×10^{-5}
ACR L	-1.44×10^{-2} [b]	2.79×10^{-5} [b]	2.90×10^{-5} [b]	2.56×10^{-5} [b]	4.35×10^{-3}	-1.71×10^{-5}	-1.68×10^{-5}	-1.79×10^{-5}
ACR R	-1.08×10^{-2} [b]	2.72×10^{-5} [b]	2.66×10^{-5} [b]	2.84×10^{-5} [b]	5.57×10^{-3}	-1.67×10^{-5}	-1.64×10^{-5}	-1.72×10^{-5}
SCR L	-1.44×10^{-2} [b]	2.80×10^{-5} [b]	2.75×10^{-5} [b]	2.89×10^{-5} [b]	-2.97×10^{-3}	-1.83×10^{-5}	-1.25×10^{-5}	-2.99×10^{-5}
SCR R	-1.46×10^{-2} [b]	2.85×10^{-5} [b]	2.73×10^{-5} [b]	3.08×10^{-5} [b]	-5.66×10^{-3}	-1.71×10^{-5}	-1.11×10^{-5}	-2.91×10^{-5}
PCR L	-9.41×10^{-3}	3.58×10^{-5} [b]	3.30×10^{-5} [b]	4.13×10^{-5} [b]	-2.15×10^{-3}	-2.12×10^{-5}	-1.72×10^{-5}	-2.91×10^{-5}
PCR R	-8.85×10^{-3}	2.97×10^{-5} [b]	2.75×10^{-5} [b]	3.42×10^{-5} [b]	-3.12×10^{-3}	-9.82×10^{-6}	-7.77×10^{-6}	-1.39×10^{-5}
PTR L	-1.57×10^{-2} [b]	2.26×10^{-5} [b]	2.64×10^{-5} [b]	1.52×10^{-5}	1.47×10^{-2}	-1.61×10^{-5}	-2.16×10^{-5}	-5.32×10^{-6}
PTR R	-1.12×10^{-2} [b]	2.74×10^{-5} [b]	2.65×10^{-5} [b]	2.92×10^{-5} [b]	9.02×10^{-3}	-1.24×10^{-5}	-1.54×10^{-5}	-6.57×10^{-6}
SS L	-1.51×10^{-2} [b]	2.04×10^{-5} [b]	2.38×10^{-5} [b]	1.37×10^{-5}	1.31×10^{-2}	-6.74×10^{-6}	-1.32×10^{-5}	6.09×10^{-6}
SS R	-9.22×10^{-3}	1.86×10^{-5} [b]	2.01×10^{-5} [b]	1.57×10^{-5}	9.51×10^{-3}	-1.14×10^{-5}	-1.52×10^{-5}	-3.80×10^{-6}
EC L	-1.00×10^{-2} [b]	2.85×10^{-5} [b]	2.82×10^{-5} [b]	2.92×10^{-5} [b]	4.70×10^{-3}	-6.32×10^{-6}	-7.72×10^{-6}	-3.50×10^{-6}
EC R	-6.82×10^{-3}[b]	2.58×10^{-5} [b]	2.44×10^{-5} [b]	2.87×10^{-5} [b]	3.03×10^{-3}	-8.24×10^{-6}	-8.91×10^{-6}	-6.89×10^{-6}
CGC L	-8.53×10^{-3}[b]	2.22×10^{-5} [b]	2.34×10^{-5} [b]	1.98×10^{-5}	3.27×10^{-3}	4.40×10^{-6}	1.43×10^{-6}	1.03×10^{-5}
CGC R	-5.91×10^{-3}	2.27×10^{-5} [b]	2.26×10^{-5} [b]	2.30×10^{-5}	3.20×10^{-3}	2.06×10^{-6}	-6.52×10^{-7}	7.49×10^{-6}
CGH L	-1.23×10^{-2} [b]	-2.19×10^{-6}	2.87×10^{-6}	-1.23×10^{-5}	3.01×10^{-3}	-9.74×10^{-7}	-3.66×10^{-6}	4.40×10^{-6}
CGH R	-5.82×10^{-3}[b]	6.72×10^{-7}	3.55×10^{-6}	-5.08×10^{-6}	3.11×10^{-3}	-2.48×10^{-6}	-4.25×10^{-6}	1.04×10^{-6}
FX/ST L	-1.17×10^{-2} [b]	1.99×10^{-5} [b]	2.30×10^{-5} [b]	1.36×10^{-5}	6.69×10^{-3}	-6.62×10^{-6}	-9.66×10^{-6}	-5.34×10^{-7}
FX/ST R	-3.22×10^{-3}	1.71×10^{-5} [b]	1.68×10^{-5} [b]	1.76×10^{-5}	8.53×10^{-3}	-4.52×10^{-6}	-7.49×10^{-6}	1.42×10^{-6}
SLF L	-9.22×10^{-3}	2.54×10^{-5} [b]	2.43×10^{-5} [b]	2.76×10^{-5} [b]	-1.42×10^{-3}	-6.37×10^{-6}	-4.07×10^{-6}	-1.10×10^{-5}
SLF R	-9.89×10^{-3}[b]	2.46×10^{-5} [b]	2.43×10^{-5} [b]	2.51×10^{-5} [b]	-2.08×10^{-3}	-4.15×10^{-6}	-2.12×10^{-6}	-8.22×10^{-6}
SFO L	-7.05×10^{-3}	3.69×10^{-5} [b]	3.22×10^{-5} [b]	4.65×10^{-5} [b]	-1.39×10^{-3}	-2.88×10^{-5}	-2.33×10^{-5}	-3.99×10^{-5}
SFO R	-9.88×10^{-3}[b]	3.13×10^{-5} [b]	2.79×10^{-5} [b]	3.80×10^{-5} [b]	-4.25×10^{-5}	-2.01×10^{-5}	-1.71×10^{-5}	-2.60×10^{-5}
IFO L	-1.47×10^{-2} [b]	3.19×10^{-5} [b]	3.32×10^{-5} [b]	2.92×10^{-5} [b]	3.10×10^{-3}	-6.20×10^{-6}	-6.92×10^{-6}	-4.76×10^{-6}
IFO R	-9.55×10^{-3}	3.08×10^{-5} [b]	2.98×10^{-5} [b]	3.28×10^{-5} [b]	3.11×10^{-3}	-5.28×10^{-6}	-6.50×10^{-6}	-2.85×10^{-6}
UNC L	-1.15×10^{-2} [b]	2.98×10^{-5} [b]	3.00×10^{-5} [b]	2.95×10^{-5} [b]	1.61×10^{-3}	-7.13×10^{-6}	-7.51×10^{-6}	-6.38×10^{-6}
UNC R	-7.74×10^{-3}	2.51×10^{-5} [b]	2.37×10^{-5} [b]	2.79×10^{-5} [b]	6.75×10^{-3}	-9.07×10^{-6}	-1.10×10^{-5}	-5.22×10^{-6}
TAP L	-1.06×10^{-2}	3.71×10^{-5} [b]	3.60×10^{-5} [b]	3.91×10^{-5} [b]	1.03×10^{-2}	-3.94×10^{-5}	-4.02×10^{-5}	-3.80×10^{-5}
TAP R	-1.67×10^{-2} [b]	6.09×10^{-5} [b]	5.70×10^{-5} [b]	6.88×10^{-5} [b]	1.15×10^{-2}	-3.37×10^{-5}	-3.51×10^{-5}	-3.09×10^{-5}

[a]Superior cerebellar peduncle on the right (R), corticospinal tract (R), inferior cerebellar peduncle (R) are not shown as they did not pass FDR in any analyses.
[b]FDR significant at $q = 0.05$ (Benjamini and Hochberg, 1995).
[c]critical FDR *p*-value.

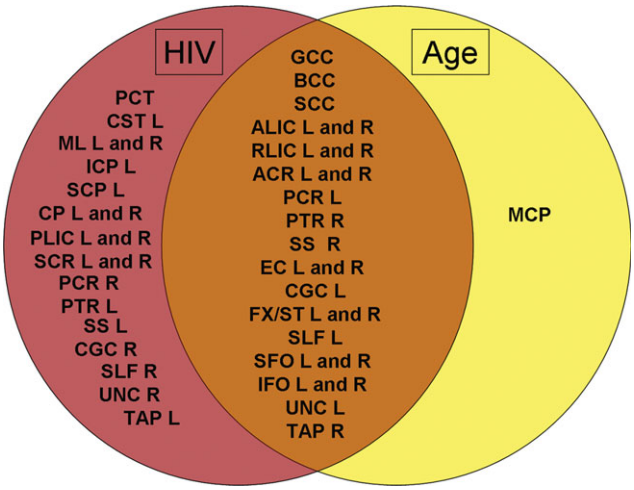

Figure 5.
Venn diagram of ROIs from the HIV diagnosis regressions that were significantly associated with the age component, HIV diagnosis component, or both across any of the DTI measures (FA, MD, RD, AD). [Color figure can be viewed in the online issue, which is available at wileyonlinelibrary.com.]

DISCUSSION

Cerebral atrophy and cognitive impairment are common in HIV-infected patients. However, whether or not such deficits can occur or persist despite widespread access to cART, and how normal age interacts with HIV infection is still largely unknown. This study had three main findings: (1) In elderly HIV+ patients, 95% of whom were on stable cART, FA was lower and diffusivity higher throughout the WM; (2) Widespread white matter aberrations were related to cognitive scores when both HIV+ and control groups were pooled, and also when the HIV+ group was considered on its own. Both NPZ and sNPZ scores showed a positive association with FA and negative association with diffusivity. These correlations were in the expected direction, as deteriorations in fiber integrity are generally accompanied by lower FA and higher values for the diffusivity measures (such as MD); (3) While we found no significant HIV by age interaction, HIV and age were both independently associated with WM deficits.

Several *post-mortem* and *in vivo* imaging approaches have previously been used to assess brain differences associated with HIV. Gray matter and white matter have long been known to be severely affected by HIV infection, but few studies have examined the effects of HIV using DTI. Early autopsy studies of HIV+ patients revealed widespread brain injury, including increased numbers of microglia, macrophages, astrocytes, and multinucleated giant cells, in the basal ganglia and deep white matter (Navia et al., 1986). Brain MRI studies show extensive atrophy of deep central gray matter structures, and the extent of atrophy is related to cognitive deficits (Aylward et al., 1993; Cohen et al., 2010a; Hall et al., 1996; Hestad et al., 1993). Cerebral metabolic disturbances, on MR spectroscopy, are also associated with lower cortical and subcortical volumes in HIV+ patients (Cohen et al., 2010b) and associated with cognitive impairment (Harezlak et al., 2011). Cortical mapping techniques also reveal selective cortical thinning in primary sensorimotor, premotor, and visual areas (Thompson et al., 2005). Our DTI results here are consistent with many MRI studies using tensor-based morphometry (TBM), surface-based anatomical maps, and other types of quantitative morphometry to show white matter atrophy in the primary and association sensorimotor regions (Chiang et al., 2007), corpus callosum thinning (Thompson et al., 2006), and corpus callosum area and width reduction (Tate et al., 2011).

Our findings agree with prior DTI studies of HIV. Many previous ROI-based DTI studies report lower FA and higher MD in the corpus callosum and frontal white matter in HIV patients (Chang et al., 2008; Filippi et al., 2001; Pfefferbaum et al., 2007; Pomara et al., 2001; Thurnher et al., 2005; Wu et al., 2006), as well as regions such as the fornix,

TABLE IV. Atlas ROI mean anisotropy and diffusivity. Here we highlight regions with the top 10 FDR significant *P*-values (greatest effect sizes) for the age component in regression analyses that included HIV status and age. FA was not significantly associated with age

			Age				
FA	*P*-value	MD	*P*-val	RD	*P*-val	AD	*P*-val
–	–	IFO L	1.62×10^{-4}	ACR L	5.28×10^{-4}	IFO L	1.80×10^{-4}
–	–	ACR L	5.68×10^{-4}	IFO L	5.61×10^{-4}	SLF L	4.18×10^{-4}
–	–	EC L	8.97×10^{-4}	ALIC L	1.08×10^{-3}	GCC	6.24×10^{-4}
–	–	SFO L	1.11×10^{-3}	EC L	1.12×10^{-3}	RLIC L	8.56×10^{-4}
–	–	UNC L	1.13×10^{-3}	SFO L	1.18×10^{-3}	EC L	1.02×10^{-3}
–	–	ALIC L	1.20×10^{-3}	UNC L	1.68×10^{-3}	ACR L	1.31×10^{-3}
–	–	ALIC R	1.67×10^{-3}	PCR L	2.27×10^{-3}	SFO L	1.35×10^{-3}
–	–	RLIC L	1.72×10^{-3}	ALIC R	2.36×10^{-3}	ACR R	1.93×10^{-3}
–	–	GCC	1.74×10^{-3}	FX/ST L	3.45×10^{-3}	UNC L	2.03×10^{-3}
–	–	PCR L	1.87×10^{-3}	GCC	4.05×10^{-3}	ALIC R	2.34×10^{-3}

TABLE V. Atlas ROI mean anisotropy and diffusivity. Here we highlight regions with the top 10 FDR significant *P*-values (greatest effect sizes) for the HIV diagnosis component in regression analyses that included HIV status and age

HIV diagnosis							
FA	*P*-value	MD	*P*-val	RD	*P*-val	AD	*P*-val
CGH L	1.91×10^{-5}	BCC	7.72×10^{-7}	BCC	1.74×10^{-6}	BCC	8.18×10^{-6}
ML L	1.03×10^{-4}	TAP R	8.23×10^{-6}	TAP R	9.47×10^{-6}	TAP R	6.07×10^{-5}
BCC	1.42×10^{-4}	IFO L	6.04×10^{-5}	SCR L	2.75×10^{-5}	IFO R	1.51×10^{-4}
CP L	2.13×10^{-4}	IFO R	8.79×10^{-5}	SCR R	2.97×10^{-5}	PCR L	1.58×10^{-4}
EC L	4.07×10^{-4}	SCR R	1.12×10^{-4}	IFO L	7.42×10^{-5}	PCR R	2.63×10^{-4}
SCP L	5.40×10^{-4}	PCR L	1.65×10^{-4}	CP L	7.91×10^{-5}	SLF. L	4.06×10^{-4}
CP R	8.02×10^{-4}	SCR L	1.72×10^{-4}	EC L	9.16×10^{-5}	PTR R	5.08×10^{-4}
SCR L	9.30×10^{-4}	EC L	1.85×10^{-4}	SFO R	1.44×10^{-4}	IFO L	6.34×10^{-4}
SCR R	1.00×10^{-3}	PTR R	2.19×10^{-4}	IFO R	2.29×10^{-4}	EC L	9.49×10^{-4}
SCC	1.83×10^{-3}	SCC	2.22×10^{-4}	CP R	2.46×10^{-4}	SCC	1.23×10^{-3}

internal and external capsules, and superior cingulate (Pfefferbaum et al., 2009). These studies have also linked lower mean FA with dementia severity (Pfefferbaum et al., 2007; Ragin et al. 2005; Wu et al., 2006). However, using pre-determined ROIs limits the scope of findings.

Recent voxel-wise analyses, such as this one, found more diffuse HIV-associated white matter deficits. Chen et al. (2009) found widespread decreases in FA and increases in MD in frontal white matter, the corpus callosum, internal capsule and *corona radiata*, and occipital white matter including the optic radiations in their voxel-based comparison of 29 HIV+ patients, (mean age: 41 years) with age-matched controls. Gongvatana et al. (2009) related loss of cognitive function in middle-aged HIV patients, to lower FA in the corpus callosum in addition to increased MD measures in the internal capsule, corpus callosum, *corona radiata*, and superior longitudinal fasciculus. Stebbins et al. (2007) found higher MD and lower FA in the subcortical WM of 30 HIV+ patients with a much younger average age of 45 years. However, they did not find significant correlations between FA and MD and cognitive performance measures. As in these prior voxel-based studies, we found lower FA and higher MD not only throughout the entire corpus callosum but also more pervasively throughout WM regions that carry commissural fibers from the corpus callosum and the projection fibers of the *corona radiata*. Like previous studies that have found NP impairment even among HIV+ patients receiving cART (Heaton et al., 2010), these WM aberrations were also associated with cognitive performance measures.

Compared to these prior VBA studies, we assessed a larger population of older subjects — over the age of 60 years. DTI studies of normal aging show age-related changes in FA in the corpus callosum, internal capsules, and white matter in all four lobes (Lehmbeck et al., 2006; Salat et al., 2005; Sullivan et al., 2001). Neurological deficits increase with age, so we might expect DTI scans to show greater and more widespread white matter deficits in elderly HIV+ patients, suggesting an age by HIV status interaction. However, we did not find an age by HIV status interaction, but found that both age and HIV independently contributed to WM deficits. This may be largely explained by the cohort's narrow age range. Figure 5 shows a large overlap in ROIs associated with both age and HIV, implying that both aging and the virus may independently cause the same brain regions to deteriorate. As seen in the *P*-values listed in Tables IV and V, the effect size for HIV status is greater (lower *P*-values) than that for age, but this may also reflect the limited age range.

Comparisons of HIV effects in young versus older subjects are limited, and it is not clear if HIV potentiates or accelerates the risk for impairment with age. Previous longitudinal MRI studies found accelerated volumetric atrophy in HIV patients relative to seronegative controls (Cardenas et al., 2009; Stout et al., 1998). Several studies report independent effects of age and HIV but have not detected any interaction — these include NP studies (Cysique et al., 2011; Scott et al., 2011; Valcour et al., 2011) and volumetric MRI studies (Ances et al., 2012; Becker et al., 2012). In a DTI study of 85 HIV+ individuals ranging from 23 to 65 years of age, Gongvatana et al. (2011) found widespread associations between FA and MD abnormalities and age throughout the WM in HIV patients, but they did not detect an interaction between age and measures of HIV infection. Another recent VBA DTI study by Towgood et al. (2012) compared young and old cohorts of HIV patients, but found no significant age by HIV status interactions. Some age effects in HIV studies may arise because age tends to be correlated with the duration of infection — as a patient lives longer, their age and duration of illness both increase. Pfefferbaum et al. (2012) found that age at HIV infection was a predictor of atrophy, whereas age alone was not an effective predictor.

The cognitive deficits associated with HIV infection, including motor coordination, information processing speed, working memory, and executive functions, support the hypothesis that HIV preferentially impairs frontal-

striatal function (Melrose et al., 2008). Many studies report deficits primarily in the frontal lobe (Cloak et al., 2004; Brito e Silva et al., 2011; Tate et al., 2009; Tucker et al., 2004). However, our findings do not fully support this localization, as we found widespread deficits throughout the brain, even in the brainstem, not isolated to frontal circuits. The strongest associations between FA loss (and diffusivity increase) and poorer NP scores were found in the body and splenium of the corpus callosum and its parieto-occipital connections, in both our DTI maps and ROI analyses. Interestingly, in another ROI based study by Wu et al. (2006), higher MD and lower FA were detected only in the splenium and not in the genu and frontal white matter; these differences were associated with dementia severity and poorer motor speed. However, DTI studies are often better powered to find deficits in regions where the FA is highest, such as the splenium and thalamic radiations. Regions with lower FA — such as the gray matter or less coherent regions of the white matter — offer poorer signal-to-noise ratios for detecting group differences, partly because the anatomy is not as consistent across subjects (Basser, 1995; Pierpaoli and Basser, 1996; Pierpaoli et al., 1996). Any variance in anatomy across subjects will make it harder to detect a consistent group difference. There may be impairments in additional white matter regions that may be undetected depending on the degree of variation in fiber organization across subjects. As such the corpus callosum often shows large effects for group differences, perhaps not only for biological reasons but also because its greater thickness and higher FA make differences easier to detect.

HIV related deficits were related more strongly to RD than to any other DTI measure, followed by MD, and cognitive scores were associated most with FA, followed by RD (Figure 1). FA tends to indicate greater fiber coherence, but MD is an overall measure of diffusion in any direction. Both FA and MD are affected by several white matter characteristics such as myelination, axonal density, and integrity (Song et al. 2005; Sun et al., 2006). AD — a measure of diffusivity along fibers — and RD — a measure of diffusion perpendicular to the axonal fibers — may reflect axonal injury and demyelination, respectively (Sun et al., 2006). Like our findings, Chen et al. (2009) found that RD was the most sensitive for detecting effects of HIV infection, suggesting that demyelination may be progressive in the white matter. In addition, Davis et al. (2009) proposed the myelin degeneration hypothesis that predicts that general age effects should be greater for RD than AD and found that both the effects of aging on white matter and their impact on cognitive performance were stronger for RD than for AD. However, a recent study by Pfefferbaum et al. (2009) found that in a group of subjects in their 40s, HIV infected individuals generally had higher axial diffusivity than controls, indicative of axonal compromise. Our results are more in line with the myelin degeneration hypothesis as we examined an older population.

In all four NPZ and sNPZ DTI maps, we found significant regions that exhibited associations with cognitive scores in a direction opposite to what would be expected. DTI has some limitations in gauging fiber integrity in regions with extensive fiber crossing and mixing. High angular diffusion imaging (HARDI) can better characterize complex intra-voxel structures than single-tensor models of DTI. A recent study showed that calculating FA from the tensor distribution function (TDF) using HARDI data better characterized the anisotropy in regions of fiber crossings (Zhan et al., 2009). Resolving the multi-fiber distribution of WM in these regions may provide a better understanding of why these regions showed an opposite association.

Findings of associations between CD4 levels and brain pathology have been mixed. A number of studies have not detected a correlation between current or nadir CD4 and brain volumes or FA (Ances et al., 2012; Becker et al., 2011; Klunder et al., 2008; Thurnher et al., 2005). However, other investigators have reported a significant correlation between nadir CD4 and regional brain volumes (Chiang et al., 2007; Cohen et al., 2010a). Interestingly, a recent study by Jernigan et al. (2011) found both that lower nadir CD4 was associated with lower gray and white matter volumes, and that higher current CD4 levels were associated with more MRI abnormality. We found no associations between measures of white matter integrity and either the nadir or current CD4 T-cell count. It may be that a larger cohort would detect these associations, or that in older cohorts with a longer duration of illness there is a decoupling of links between the level of white matter impairment and past measures of T-cell counts. These links deserve further exploration.

This study also has some limitations. The lack of a young comparison group limits the scientific and clinical significance of the study somewhat. Future studies are needed to contrast elderly people and younger people with HIV. Also, longitudinal studies would be better able to relate age effects on DTI to neuropsychiatric and cognitive measures in the same individuals. The large size of our NP test battery led us to summarize over-all NP testing performance in one summary score rather than attempt to investigate domain-specific scores. Although there are potential pitfalls if one or more test excessively contributes to the summary score due to skewed distribution with outliers, we took the precaution of examining the distributions prior to combining them. While this is a simplified approach, we believe it is valid with the precautions that we have taken. Alternate investigations could focus on specific NP domains, or combine different ones using a predetermined weighting scheme.

In conclusion, elderly HIV+ patients showed widespread disruptions of projection, association, and commissural tracts, relative to controls and these disruptions are associated with NP deficits. While we did not examine the effect of age by including a younger cohort in this study, our maps implicate widespread regions, and may indicate the compounded effects of aging, as proposed before in the context

of HIV (Ances et al., 2012; Kirk and Goetz, 2009; Valcour et al., 2004a,b). HIV infection has transitioned to a chronic geriatric disease with HIV+ patients living longer due to widespread availability of cART; yet, they continue to experience a greater burden of neurological abnormalities when compared to age-matched healthy counterparts. Co-morbidities, including cerebrovascular and neurodegenerative phenomena as well as the effects of normal aging may be further complicated by HIV infection. Future work with larger aging cohorts and other imaging methods may complement these findings, and help in understanding the symptoms and prognosis for patients with HIV.

ACKNOWLEDGMENTS

This study was supported by the following grants: K23AG032872 (to V.V.), P50 AG023501 (ADRC, PI: Bruce Miller); P30-AI027763 (UCSF CFAR), UL1 RR024131 (UCSF GCRC), the Larry L. Hillblom Foundation and the AIDS Research Institute at UCSF. T.N., N.J., and P.T. were supported in part by the National Institute for Biological Imaging and Bioengineering (R01 EB008432, R01 EB007813, and P41 RR013642 to PT). NJ was supported in part by NIH NLM Grant T15 LM07356.

REFERENCES

Ances BM, Ellis RJ (2007): Dementia and neurocognitive disorders due to HIV-1 infection. Semin Neurol 27:86–92.

Ances BM, Ortega M, Vaida F, Heaps J, Paul R (2012): Independent effects of HIV, aging, and HAART on brain volumetric measures. J Acquir Immune Defic Syndr 59:469–477.

Assaf Y, Basser PJ (2005): Composite hindered and restricted model of diffusion (CHARMED) MR imaging of the human brain. NeuroImage 27:48–58.

Aylward EH, Henderer JD, McArthur JC, Brettschneider PD, Harris GJ, Barta PE, Pearlson GD (1993): Reduced basal ganglia volume in HIV-1-associated dementia: Results from quantitative neuroimaging. Neurology 43:2099–2104.

Basser PJ, Mattiello J, Le Bihan D (1994): MR diffusion tensor spectroscopy and imaging. Biophys J 66:259–267.

Basser PJ (1995): Inferring microstructural features and the physiological state of tissues from diffusion-weighted images. NMR Biomed 8:333–344.

Becker JT, Sanchez J, Dew MA, Lopez OL, Dorst SK, Banks G (1997): Neuropsychological abnormalities among HIV-infected individuals in a community-based sample. Neuropsychology 11:592–601.

Becker JT, Kingsley L, Mullen J, Cohen B, Martin E, Miller EN, Ragin A, Sacktor N, Selnes OA, Visscher BR (2009): Vascular risk factors, HIV serostatus, and cognitive dysfunction in gay and bisexual men. Neurology 73:1292–1299.

Becker JT, Sanders J, Madsen SK, Ragin A, Kingsley L, Maruca V, Cohen B, Goodkin K, Martin E, Miller EN, Sacktor N, Alger JR, Barker PB, Saharan P, Carmichael OT, Thompson PM (2011): Subcortical brain atrophy persists even in HAART-regulated HIV disease. Brain Imaging Behav 5:77–85.

Becker JT, Maruca V, Kingsley LA, Sanders JM, Alger JR, Barker PB, Goodkin K, Martin E, Miller EN, Ragin A, Sacktor N, Selnes O (2012): Factors affecting brain structure in men with HIV disease in the post-HAART era. Neuroradiology 54:113–121.

Benjamini Y, Hochberg Y (1995): Controlling the false discovery rate – A practical and powerful approach to multiple testing. J Roy Statis Soc Ser B-Method 57:289–300.

Brew BJ, Crowe SM, Landay A, Cysique LA, Guillemin G (2009): Neurodegeneration and ageing in the HAART era. J Neuroimmune Pharmacol 4:163–174.

Brito e Silva ET, Caixeta LF, Soares VL, Sagawa GR (2011): HIV-associated dementia in older adults: Clinical and tomographic aspects. Int Psychogeriatr 23:1061–1069.

Brun CC, Lepore N, Pennec X, Chou YY, Lopez OL, Aizenstein HJ, Becker JT, Toga AW, Thompson PM (2007): Comparison of standard and riemannian elasticity for tensor-based morphometry in HIV/AIDS. MICCAI 2007 Workshop on Image Registration.

Buckner RL (2004): Memory and executive function in aging and AD: Multiple factors that cause decline and reserve factors that compensate. Neuron 44:195–208.

Cardenas VA, Meyerhoff DJ, Studholme C, Kornak J, Rothlind J, Lampiris H, Neuhaus J, Grant RM, Chao LL, Truran D, Weiner MW (2009): Evidence for ongoing brain injury in human immunodeficiency virus-positive patients treated with antiretroviral therapy. J Neurovirol 15:324–333.

Carpenter CC, Cooper DA, Fischl MA, Gatell JM, Gazzard BG, Hammer SM, Hirsch MS, Jacobsen DM, Katzenstein DA, Montaner JS, Richman DD, Saag MS, Schechter M, Schooley RT, Thompson MA, Vella S, Yeni PG, Volberding PA (2000): Antiretroviral therapy in adults: Updated recommendations of the International AIDS Society–USA Panel. JAMA 283:381–390.

Chang L, Wong V, Nakama H, Watters M, Ramones D, Miller EN, Cloak C, Ernst T (2008): Greater than age-related changes in brain diffusion of HIV patients after 1 year. J Neuroimmune Pharmacol 3:265–274.

Chen Y, An H, Stone T, Smith JK, Hall C, Bullitt E, Shen D, Lin W (2009): White matter abnormalities revealed by diffusion tensor imaging in non-demented and demented HIV patients. Neuroimage 47:1154–1162.

Cherner M, Ellis RJ, Lazzaretto D, Young C, Mindt MR, Atkinson JH, Grant I, Heaton RK (2004): Effects of HIV-1 infection and aging on neurobehavioral functioning: Preliminary findings. AIDS 18:S27–S34.

Chiang MC, Dutton RA, Hayashi KM, Toga AW, Lopez OL, Aizenstein HJ, Toga AW, Becker JT, Thompson PM (2007): 3D pattern of brain atrophy in HIV/AIDS visualized using tensor-based morphometry. Neuroimage 34:44–60.

Cloak CC, Chang L, Ernst T (2004): Increased frontal white matter diffusion is associated with glial metabolites and psychomotor slowing in HIV. J Neuroimmunol 157:147–152.

Cohen RA, Harezlak J, Schifitto G, Hana G, Clark U, Gongvatana A, Paul R, Taylor M, Thompson P, Alger J, Brown M, Zhong J, Campbell T, Singer E, Daar E, McMahon D, Tso Y, Yiannoutsos CT, Navia B (2010a): Effects of nadir CD4 count and duration of human immunodeficiency virus infection on brain volumes in the highly active antiretroviral therapy era. J Neurovirol 16:25–32.

Cohen RA, Harezlak J, Gongvatana A, Buchthal S, Schifitto G, Clark U, Paul R, Taylor M, Thompson P, Tate D, Alger J, Brown M, Zhong J, Campbell T, Singer E, Daar E, McMahon D, Tso Y, Yiannoutsos CT, Navia B (2010b): Cerebral metabolite abnormalities in human immunodeficiency virus are associated with cortical and subcortical volumes. J Neurovirol 16:435–444.

Cysique LA, Maruff P, Brew BJ (2006): Variable benefit in neuropsychological function in HIV-infected HAART-treated patients. Neurology 66:1447–1450.

Cysique LA, Maruff P, Bain MP, Wright E, Brew BJ (2011): HIV and age do not substantially interact in HIV-associated neurocognitive impairment. J Neuropsychiatry Clin Neurosci 23:83–89.

Davis SW, Dennis NA, Buchler NG, White LE, Madden DJ, Cabeza R (2009): Assessing the effects of age on long white matter tracts using diffusion tensor tractography. Neuroimage 46:530–541.

Douaud G, Jbabdi S, Behrens TE, Menke RA, Gass A, Monsch AU, Rao A, Whitcher B, Kindlmann G, Matthews PM, Smith S, (2011): DTI measures in crossing-fibre areas: Increased diffusion anisotropy reveals early white matter alteration in MCI and mild Alzheimer's disease. Neuroimage 55:880–890.

Filippi CG, Ulug AM, Ryan E, Ferrando SJ, van Gorp W (2001): Diffusion tensor imaging of patients with HIV and normal-appearing white matter on MR images of the brain. Am J Neuroradiol 22:277–283.

Glisky EL (2007): Changes in cognitive function in human aging. In: Riddle DR, editor. Brain Aging: Models, Methods and Mechanisms. Boca Raton (FL): CRC Press. Chapter 1. pp. 3–20.

Goodkin K, Wilkie FL, Concha M, Hinkin CH, Symes S, Baldewicz TT, Asthana D, Fujimura RK, Lee D, van Zuilen MH, Khamis I, Shapshak P, Eisdorfer C (2001): Aging and neuroAIDS conditions and the changing spectrum of HIV-1-associated morbidity and mortality. J Clin Epidem 54:S35–S43.

Gongvatana A, Schweinsburg BC, Taylor MJ, Theilmann RJ, Letendre SL, Alhassoon OM, Jacobus J, Woods SP, Jernigan TL, Ellis RJ, Frank LR, Grant I (2009): White matter tract injury and cognitive impairment in human immunodeficiency virus-infected individuals. J Neurovirol 15:187–195.

Gongvatana A, Cohen RA, Correia S, Devlin KN, Miles J, Kang H, Ombao H, Navia B, Laidlaw DH, Tashima KT (2011): Clinical contributors to cerebral white matter integrity in HIV-infected individuals. J Neurovirol 17:477–486.

Gutman B, Svarer C, Leow AD, Yanovsky I, Toga AW, Thompson PM (2010): Creating Unbiased Minimal Deformation Templates for Brain Volume Registration. Barcelona, Spain: OHBM.

Hall M, Whaley R, Robertson K, Hamby S, Wilkins J, Hall C (1996): The correlation between neuropsychological and neuroanatomic changes over time in asymptomatic and symptomatic HIV-1-infected individuals. Neurology 46:1697–1702.

Harezlak J, Buchthal S, Taylor M, Schifitto G, Zhong J, Daar E, Alger J, Singer E, Campbell T, Yiannoutsos C, Cohen R, Navia B (2011): Persistence of HIV-associated cognitive impairment, inflammation, and neuronal injury in era of highly active antiretroviral treatment. AIDS 25:625–633.

Hartley A (2006): Changing role of the speed of processing construct in the cognitive psychology of human aging. In: Birren JE, Schaiere KW, editors. Handbook of the Psychology of Aging. Amsterdam, Netherlands: Elsevier. pp 183–207.

Heaton RK, Clifford DB, Franklin DR, Woods SP, Ake C, Vaida F, Ellis RJ, Letendre SL, Marcotte TD, Atkinson JH, Rivera-Mindt M, Vigil OR, Taylor MJ, Collier AC, Marra CM, Gelman BB, McArthur JC, Morgello S, Simpson DM, McCutchan JA, Abramson I, Gamst A, Fennema-Notestine C, Jernigan TL, Wong J, Grant I (2010): HIV-associated neurocognitive disorders persist in the era of potent antiretroviral therapy: CHARTER Study. Neurology 75:2087–2096.

Heaton RK, Franklin DR, Ellis RJ, McCutchan JA, Letendre SL, Leblanc S, Corkran SH, Duarte NA, Clifford DB, Woods SP, Collier AC, Marra CM, Morgello S, Mindt MR, Taylor MJ, Marcotte TD, Atkinson JH, Wolfson T, Gelman BB, McArthur JC, Simpson DM, Abramson I, Gamst A, Fennema-Notestine C, Jernigan TL, Wong J, Grant I (2011): HIV-associated neurocognitive disorders before and during the era of combination antiretroviral therapy: Differences in rates, nature, and predictors. J Neurovirol 17:3–16.

Heflin LH, Laluz V, Jang J, Ketelle R, Miller BL, Kramer JH (2011): Let's inhibit our excitement: The relationships between Stroop, behavioral disinhibition, and the frontal lobes. Neuropsychology 25:655–665.

Hestad K, McArthur JH, Dal Pan GJ, Selnes OA, Nance-Sproson TE, Aylward E, Mathews VP, McArthur JC (1993): Regional brain atrophy in HIV-1 infection: Association with specific neuropsychological test performance. Acta Neurol Scand 88:112–118.

Holmes CJ, Hoge R, Collins L, Woods R, Toga AW, Evans AC (1998): Enhancement of MR images using registration for signal averaging. J Comput Assist Tomogr 22:324–333.

Holt JL, Kraft-Terry SD, Chang L (2012): Neuroimaging studies of the aging HIV-1-infected brain. J Neurovirol 18:291–302.

Iglesias JE, Liu CY, Thompson P, Tu Z (2011): Robust brain extraction across datasets and comparison with publicly available methods. IEEE Trans Med Imag 30:1617–1634.

Jahanshad N, Lee AD, Barysheva M, McMahon KL, de Zubicaray GI, Martin NG, Wright MJ, Toga AW, Thompson PM (2010): Genetic influences on brain asymmetry: A DTI study of 374 twins and siblings. Neuroimage 52:455–469.

Jenkinson M, Bannister P, Brady J, Smith S (2002): Improved optimisation for the robust and accurate linear registration and motion correction of brain images. NeuroImage 17:825–841.

Jernigan TL, Archibald SL, Fennema-Notestine C, Taylor MJ, Theilmann RJ, Julaton MD, Notestine RJ, Wolfson T, Letendre SL, Ellis RJ, Heaton RK, Gamst AC, Franklin DR Jr, Clifford DB, Collier AC, Gelman BB, Marra C, McArthur JC, McCutchan JA, Morgello S, Simpson DM, Grant I (2011): Clinical factors related to brain structure in HIV: The CHARTER study. J Neurovirol 17:248–257.

Kirk JB, Goetz MB (2009): Human immunodeficiency virus in an aging population, a complication of success. J Am Geriatr Soc 57:2129–2138.

Kissel EC, Pukay-Martin ND, Bornstein RA (2005): The relationship between age and cognitive function in HIV-infected men. J Neuropsychiatry Clin Neurosci 17:180–184.

Klunder AD, Chiang MC, Dutton RA, Lee SE, Toga AW, Lopez OL, Aizenstein HJ, Becker JT, Thompson PM (2008): Mapping cerebellar degeneration in HIV/AIDS. NeuroReport 19: 1655–1659.

Kramer JH, Jurik J, Sha SJ, Rankin KP, Rosen HJ, Johnson JK, Miller BL (2003): Distinctive neuropsychological patterns in frontotemporal dementia, semantic dementia, and Alzheimer disease. Cogn Behav Neurol 16:211–218.

Kramer JH, Mungas D, Reed BR, Wetzel ME, Burnett MM, Miller BL, Weiner MW, Chui HC (2007): Longitudinal MRI and cognitive change in healthy elderly. Neuropsychology 21:412–418.

Kuroki N, Kubicki M, Nestor PG, Salisbury DF, Park HJ, Levitt JJ, Woolston S, Frumin M, Niznikiewicz M, Westin CF, Maier SE, McCarley RW, Shenton ME (2006): Fornix integrity and hippocampal volume in male schizophrenic patients. Biol Psychiatry 60:22–31.

Langers DR, Jansen JF, Backes WH (2007): Enhanced signal detection in neuroimaging by means of regional control of the global false discovery rate. Neuroimage 38:43–56.

Lee JE, Chung MK, Lazar M, DuBray MB, Kim J, Bigler ED, Lianhart JE, Alexander AL (2009): A study of diffusion tensor imaging by tissue-specific, smoothing-compensated voxel-based analysis. Neuroimage 44:870–883.

Lee DY, Fletcher E, Carmichael OT, Singh B, Mungas D, Reed B, Martinez O, Buonocore MH, Persianinova M, DeCarli C (2012): Sub-regional hippocampal injury is associated with fornix degeneration in alzheimer's disease. Front Aging Neurosci 4:1 [online only].

Lehmbeck JT, Brassen S, Weber-Fahr W, Braus DF (2006): Combining voxel-based morphometry and diffusion tensor imaging to detect age-related brain changes. Neuroreport 17:467–470.

Leow AD, Yanovsk I, Chiang MC, Lee AD, Klunder A, Lu A, Becker J, Davis S, Toga AW, Thompson PM (2007): Statistical properties of Jacobian maps and the realization of unbiased large-deformation nonlinear image registration. IEEE Trans Med Imag 26:822–832.

Lepore N, Brun CC, Pennec X, Chou YY, Lopez OL, Aizenstein HJ, Becker JT, Toga AW, Thompson PM (2007): Mean template for tensor-based morphometry using deformation tensors. MICCAI 10:826–833.

Lepore N, Brun CC, Chou YY, Chiang MC, Dutton RA, Hayashi KM, Lu A, Lopez OL, Aizenstein HJ, Toga AW, Becker JT, Thompson PM (2008): Generalized tensor-based morphometry of HIV/AIDS using multivariate statistics on deformation tensors. IEEE Trans Med Imag 27:129–141.

McArthur JC, Haughey N, Gartner S, Conant K, Pardo C, Nath A, Sacktor N (2003): Human immunodeficiency virus-associated dementia: An evolving disease. J Neurovirol 9:205–221.

McArthur JC (2004): HIV dementia: An evolving disease. J Neuroimmunol 157:3–10.

Melrose RJ, Tinaz S, Castelo JM, Courtney MG, Stern CE (2008): Compromised fronto-striatal functioning in HIV: An fMRI investigation of semantic event sequencing. Behav Brain Res 188:337–347.

Mori S, Oisha K, Jiang H, Jiang L, Li X, Kazi A, Hua K, Faria AV, Mahmood A, Woods R, Toga AW, Pike GB, Neto PR, Evans A, Zhang J, Huang H, Miller MI, Zijl P, Mazziotta J (2008): Stereotaxic white matter atlas based on diffusion tensor imaging in an ICBM template. Neuroimage 40:570–582.

Navia BA, Cho ES, Petito CK, Price RW (1986): The AIDS dementia complex: II. Neuropathology. Ann Neurol 19:525–535.

Oishi K, Faria A, van Zijl PCM, Mori S. 2011. MRI atlas of human white matter, second edition. Amsterdam: Elsevier.

Peavy G, Jacobs D, Salmon D, Butters N, Delis D, Taylor M, Massman P, Stout J, Heindel W, Kirson D, Atkinson J, Chandler J, Grant I (1994): Verbal memory performance of patients with human immunodeficiency virus infection: Evidence of subcortical dysfunction. J Clin Exp Neuropsych 16:508–523.

Pfefferbaum A, Rosenbloom MJ, Adalsteinsson E, Sullivan EV (2007): Diffusion tensor imaging with quantitative fibre tracking in HIV infection and alcoholism comorbidity: Synergistic white matter damage. Brain 130:48–64.

Pfefferbaum A, Rosenbloom MJ, Rohlfing T, Kemper CA, Deresinski S, Sullivan EV (2009): Frontostriatal fiber bundle compromise in HIV infection without dementia. AIDS 23:1977–1985.

Pfefferbaum A, Rosenbloom MJ, Sassoon SA, Kemper CA, Deresinski S, Rohlfing T, Sullivan EV (2012): Regional brain structural dysmorphology in human immunodeficiency virus infection: Effects of acquired immune deficiency syndrome, alcoholism, and age. Biol Psychiatry 72:361–370.

Pierpaoli C, Jezzard P, Basser PJ, Barnett A, Di Chiro G (1996): Diffusion tensor MR imaging of the human brain. Radiology 201:637–648.

Pierpaoli C, Basser PJ (1996): Toward a quantitative assessment of diffusion anisotropy. Magn Reson Med 36:893–906.

Pomara N, Crandall DT, Choi SJ, Johnson G, Lim KO (2001): White matter abnormalities in HIV-1 infection: A diffusion tensor imaging study. Psychiatry Res 106:15–24.

Possin KL, Laluz V, Alcantar O, Miller BL, Kramer JH (2011): Distinct neuroanatomical substrates and cognitive mechanisms of figure copy performance in Alzheimer's disease and behavioral variant frontotemporal dementia. Neuropsychologia 49:43–48.

Ragin AB, Wu Y, Storey P, Cohen BA, Edelman RR, Epstein LG (2005): Diffusion tensor imaging of subcortical brain injury in patients infected with human immunodeficiency virus. J Neurovirol 11:292–298.

Rapport LJ, Millis SR, Bonello PJ (1998): Validation of the Warrington theory of visual processing and the visual object and space perception battery. J Clin Exp Neuropsychol 20: 211–220.

Raz N, Rodrigue KM (2006): Differential aging of the brain: Patterns, cognitive correlates and modifiers. Neurosci Biobehav Rev 30:730–748.

Ruff RM, Parker SB (1993): Gender- and age-specific changes in motor speed and eye-hand coordination in adults: Normative values for the Finger Tapping and Grooved Pegboard tests. Percept Mot Skills 76:1219–1230.

Sacktor N, McDermott MP, Marder K, Schifitto G, Selnes OA, McArthur JC, Stern Y, Albert S, Palumbo D, Kieburtz K, De Marcaida JA, Cohen B, Epstein L (2002): HIV associated cognitive impairment before and after the advent of combination therapy. J Neurovirol 8:136–142.

Salat DH, Tuch DS, Greve DN, van der Kouwe AJW, Hevelone ND, Zaleta AK, Rosen BR, Fischl B, Corkin S, Rosas HD, Dale AM (2005): Age-related alterations in white matter microstructure measured by diffusion tensor imaging. Neurobiol of Aging 26:1215–1227.

Schouten J, Cinque P, Gisslen M, Reiss P, Portegies P (2011): HIV-1 infection and cognitive impairment in the cART era: A review. AIDS 25:561–575.

Scott J, Woods S, Carey C, Weber E, Bondi M, Grant I (2011): Neurocognitive consequences of HIV infection in older adults: An evaluation of the "cortical" hypothesis. AIDS Behav 15:1187–1196.

Smith SM (2002): Fast robust automated brain extraction. Hum Brain Mapp 17:143–155.

Song SK, Yoshino J, Le TQ, Lin SJ, Sun SW, Cross AH, Armstrong RC (2005): Demyelination increases radial diffusivity in corpus callosum of mouse brain. Neuroimage 26:132–140.

Stebbins GT, Smith CA, Bartt RE, Kessler HA, Adeyemi OM, Martin E, Cox JL, Bammer R, Moseley ME (2007): HIV-associated alterations in normal-appearing white matter: A voxel-wise diffusion tensor imaging study. J Acquir Immune Defic Syndr 46:564–573.

Stout JC, Ellis RJ, Jernigan TL, Archibald SL, Abramson I, Wolfson T, McCutchan JA, Wallace MR, Atkinson JH, Grant I (1998): Progressive cerebral volume loss in human immunodeficiency virus infection: A longitudinal volumetric magnetic resonance imaging study. Arch Neurol 55:161–168.

Sullivan EV, Adalsteinsson E, Hedehus M, Ju C, Moseley M, Lim KO, Pfefferbaum A (2001): Equivalent disruption of regional

white matter microstructure in ageing healthy men and women. Neuroreport 12:99–104.

Sun SW, Liang HF, Trinkaus K, Cross AH, Armstrong RC, Song SK (2006): Noninvasive detection of cuprizone induced axonal damage and demyelination in the mouse corpus callosum. Magn Reson Med 55:302–308.

Tate DF, Conley JJ, Meier SD, Navia BA, Cohen R, Guttmann CRG (2009): Neuroimaging among HIV-infected patients: Current knowledge and future directions. In: Paul RH, editor. HIV and the Brain. New York: Humana Press. pp 75–107.

Tate DF, Sampat M, Harezlak J, Fiecas M, Hogan J, Dewey J, McCaffrey D, Branson D, Russell T, Conley J, Taylor M, Schifitto G, Zhong J, Daar ES, Alger J, Brown M, Singer E, Campbell T, McMahon D, Tso Y, Matesan J, Letendre S, Paulose S, Gaugh M, Tripoli C, Yiannoutsos C, Bigler ED, Cohen RA, Guttmann CR, Navia B (2011): Regional areas and widths of the midsagittal corpus callosum among HIV-infected patients on stable antiretroviral therapies. J Neurovirol 17:368–379.

Thompson PM, Dutton RA, Hayashi KM, Toga AW, Lopez OL, Aizenstein HJ, Becker JT (2005): Thinning of the cerebral cortex visualized in HIV/AIDS reflects CD4 T lymphocyte decline. PNAS 102:15647–15652.

Thompson PM, Dutton RA, Hayashi KM, Lu A, Lee SE, Lee JY, Lopez OL, Aizenstein HJ, Toga AW, Becker JT (2006): 3D mapping of ventricular and corpus callosum abnormalities in HIV/AIDS. NeuroImage 31:12–23.

Thurnher MM, Castillo M, Stadler A, Rieger A, Schmid B, Sundgren PC (2005): Diffusion-tensor MR imaging of the brain in human immunodeficiency virus-positive patients. Am J Neuroradiol 26:2275–2281.

Towgood KJ, Pitkanen M, Kulasegaram R, Fraderaa A, Kumara A, Sonic S, Sibtaind NA, Reeda L, Bradbeerc C, Barkera GJ, Kopelman MD (2012): Mapping the brain in younger and older asymptomatic HIV-1 men: Frontal volume changes in the absence of other cortical or diffusion tensor abnormalities. Cortex 48:230–241.

Tucker KA, Robertson KR, Lin W, Smith JK, An H, Chen Y, Aylward SR, Hall CD (2004): Neuroimaging in human immunodeficiency virus infection. J Neuroimmunol 157:153–162.

UNAIDS, 2010. UNAIDS report on the global AIDS epidemic. http://www.unaids.org/globalreport/documents/20101123_GlobalReport_full_en.pdf

Valcour V, Sacktor N (2004a): HIV-associated dementia and aging. In: Emlet CA, editor. HIV/AIDS in Older Adults. New York: Springer Publishing Company. pp 55–71.

Valcour V, Shikuma C, Shiramizu B, Watters M, Poff P, Selnes O, Holck P, Grove J, Sacktor N (2004b): Higher frequency of dementia in older HIV-1 individuals: The Hawaii Aging with HIV-1 Cohort. Neurology 63:822–827.

Valcour V, Shikuma CM, Shiramizu BT, Williams AE, Watters MR, Poff PW, Grove JS, Selnes OA, Sacktor NC (2005): Diabetes, insulin resistance, and dementia among HIV-1-infected patients. J Acquir Immune Defic Syndr 38:31–36.

Valcour V, Paul R, Neuhaus J, Shikuma C (2011): The effects of age and HIV on neuropsychological performance. J Int Neuropsychol Soc 17:190–195.

Vance DE (2010): Aging with HIV: Clinical considerations for an emerging population. Am J Nurs 110:42–47.

Wang YL, Zhang J, Gutman B, Chan TF, Becker JT, Aizenstein HJ, Lopez OL, Tamburo RJ, Toga AW, Thompson PM (2010): Multivariate tensor-based morphometry on surfaces: Application to mapping ventricular abnormalities in HIV/AIDS. NeuroImage 49:2141–2157.

Wedeen VJ, Hagmann P, Tseng WY, Reese TG, Weisskoff RM (2005): Mapping complex tissue architecture with diffusion spectrum magnetic resonance imaging. MRM 54:1377–1386.

Weintraub S, Salmon D, Mercaldo N, Ferris S, Graff-Radford NR, Chui H, Cummins J, DeCarli C, Foster NL, Galasko D, Perkind E, Dietrich W, Beekly DL, Kukull WA, Morris JC (2009): The Alzheimer's Disease Centers' Uniform Data Set (UDS): The neuropsychologic test battery. Alzheimer Dis Assoc Disord 23:91–101.

Wendelken LA, Valcour V (2012): Impact of HIV and aging on neuropsychological function. J of NeuroVirology 18:256–263.

Woods SP, Carey CL, Ludicello JE, Letendre SL, Grant I (2009): Neuropsychological aspects of HIV infection. In: Grant I, Adams KM, editors. Neuropsychological Assessment of Neuropsychiatric Disorders. New York: Oxford University Press. pp 366–397.

Wu Y, Storey P, Cohen BA, Epstein LG, Edelman RR, Ragin AB (2006): Diffusion alterations in corpus callosum of patients with HIV. Am J Neuroradiol 27:656–660.

Yanovsky I, Thompson PM, Osher S, Leow AD (2007): Topology preserving log-unbiased nonlinear image registration: Theory and implementation. IEEE Conference on Computer Vision and Pattern Recognition. pp 1–8.

Zhan L, Leow AD, Zhu S, Chiang MC, Barysheva M, Toga AW, McMahon KL, de Zubicaray GI, Wright MJ, Thompson PM (2009): Analyzing multi-fiber reconstruction in high angular resolution diffusion imaging using the tensor distribution function. IEEE International Symposium on Biomedical Imaging: From Nano to Macro. pp 1402–1405.

Zhan L, Leow AD, Aganj I, Lenglet C, Sapiro G, Yacoub E, Harel N, Toga AW, Thompson PM (2011): Differential information content in staggered multiple shell HARDI measured by the tensor distribution function, IEEE International Symposium on Biomedical Imaging: From Nano to Macro. pp 305–309.